

Considerations for Polarimetric Upgrades to Operational WSR-88D Radars

R. J. DOVIK

National Severe Storms Laboratory, Norman, Oklahoma

V. BRINGI

Colorado State University, Fort Collins, Colorado

A. RYZHKOV

Cooperative Institute of Mesoscale Meteorological Studies, University of Oklahoma, Norman, Oklahoma

A. ZAHRAI AND D. ZRNIĆ

National Severe Storms Laboratory, Norman, Oklahoma

(Manuscript received 8 October 1998, in final form 3 May 1999)

ABSTRACT

This paper reports on the steps taken by the National Severe Storms Laboratory (NSSL) to 1) develop open system hardware to facilitate upgrades to the WSR-88D (NEXRAD) radar and 2) improve identification of the type of precipitation and its quantitative measure. An engineering evaluation is made to determine if the WSR-88D antenna assembly with minimum modification could be used in a polarimetric mode. The polarimetric characteristics and radiation patterns of a research WSR-88D are briefly discussed. Considerations for the choice of polarimetric basis and design options are described. A polarimetric scheme employing simultaneous transmission of horizontally (H) and vertically (V) polarized waves is suggested for the WSR-88D, which eliminates an expensive, high-power switch. A theoretical evaluation is performed to determine the effects that feed alignment, drop canting, and backscatter depolarization have on the measurements of polarimetric parameters made with simultaneous transmission and reception of H and V signals. Experiments with the Colorado State University–Universities of Chicago and Illinois radar are performed to compare polarimetric variables obtained with alternate and simultaneous transmissions of H, V waves. Both simultaneous reception in two receivers and alternate reception in one receiver have been used.

1. Introduction

In 1997 the National Weather Service (NWS) completed the deployment of 165 meteorological radars (i.e., NEXRAD, now called the WSR-88D) that compose the U.S. network. This deployment is part of a larger effort to improve and modernize the U.S. weather service. Although the WSR-88D is a sophisticated, computer-driven radar and is a considerable improvement over the previous one based on 1950s technology, the WSR-88D employs 1980s proprietary computer technology that is already outdated and impedes incremental improvements in hardware and software. Furthermore, experience has made evident the limitations in the performance of this advanced weather radar, and recent research suggests improvements can be made.

Currently, the NWS and the National Severe Storms Laboratory (NSSL) are engaged in a project [the NEXRAD Product Improvement (NPI) project; Saffle 1997] to upgrade the WSR-88D to meet new requirements and to respond in a cost-effective manner to advances in meteorological science and technology. The NWS provided radar components that made possible the assembly of a research WSR-88D. This National Oceanic and Atmospheric Administration (NOAA)–NSSL research WSR-88D is called KOUN and is used for developing advanced radar techniques and enhancing operations. This R&D radar, located on the grounds of the University of Oklahoma, is accessible to researchers to test and evaluate new ideas in hardware and software, which have potential for implementation on the network of operational radars to improve the weather service.

2. The move to open systems

The WSR-88D consists of three functional systems: the Radar Data Acquisition (RDA), the Radar Product

Corresponding author address: Dr. Richard J. Doviak, National Severe Storms Laboratory, 1313 Halley Circle, Norman, OK 73069.
E-mail: doviak@nssl.noaa.gov

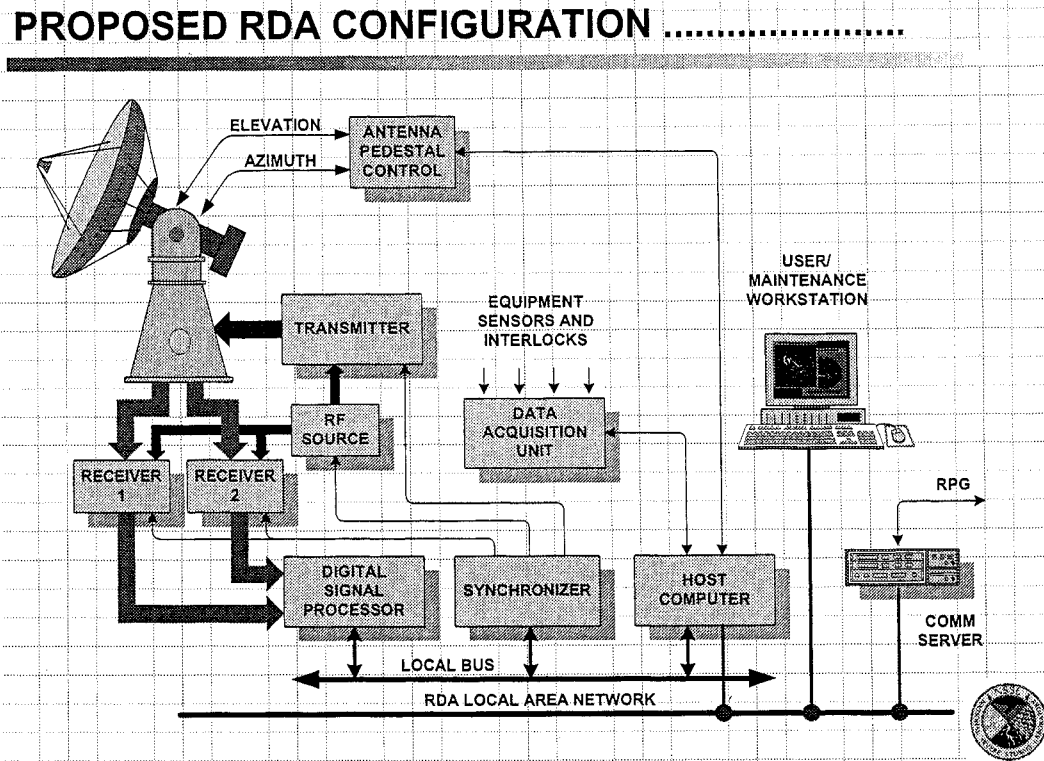


FIG. 1. A simplified block diagram of the proposed WSR-88D's Open Radar Data Acquisition unit to accommodate polarimetric upgrades.

Generator (RPG), and the Principal User Processor (PUP). The RDA contains the radar transmitter and receiver, the antenna, and a signal processor that generates the base data (i.e., the reflectivity, velocity, and spectrum width fields) used by the RPG. The RDA can be several tens of kilometers away from the Weather Forecast Office (WFO) where the RPG and PUP are housed. The RPG controls the RDA through a Unit Control Position (UCP) and provides computer analyses of the base data fields to assist the meteorologist. The RPG has over a dozen algorithms that build meteorologically useful products such as those to estimate rainfall, locate tornadoes, track storms and project their paths, profile wind, etc. It also distributes these products to external users (e.g., the National Centers for Environmental Prediction, other WFOs, River Forecast Centers, added-value vendors, etc.). The PUP is an interactive computer graphic system where the meteorologist can display the various data fields and products generated by the RPG.

The NPI project aims to improve each of the functional systems of the WSR-88D using modern, commercial-off-the-shelf (COTS) equipment and international standards for hardware and software with which products and modules from different vendors can interoperate. This aim is being achieved by using COTS equipment to develop and test hardware and software on KOUN. The design goals of the open system distributed architecture have several objectives (Zahrai and

Zrnić 1997). For example, the architecture must readily accommodate modular replacement and incremental upgrades and evolve with new standards and technologies. Applications software should be designed to be portable, at least at the source level and, if necessary, allow its migration to different hardware platforms to preserve the investment in software development.

The impetus for developing an Open RDA (ORDA) is to allow improvements in transmitter waveform design that can 1) mitigate the effects of range/velocity ambiguities (Sachidananda et al. 1997, 1998), 2) allow better management in the use of the ground clutter canceler, and 3) accommodate potential polarimetric upgrades. The present RDA unit is based on a signal processor and other subsystem components whose proprietary nature makes systematic replacement and incremental upgrades extremely difficult (Zahrai et al. 1998). The planned ORDA must not only allow for cost-effective incremental upgrades but also maintain all of the present capabilities of the WSR-88D. That is, with the exception of enhancements, the changes to the system must be transparent to the users.

Primary components of the planned ORDA configuration are presented in Fig. 1. To obtain polarimetric data, we plan to simultaneously transmit both horizontally and vertically polarized pulses and receive the co-polarized echoes in two parallel receivers (Seliga and Bringi 1976; Zrnić 1996). The receivers use fast auto-

matic gain control (AGC) circuitry and provide 12-bit, in phase (I) and quadrature phase (Q) data with 6-bit AGC attenuation values at $1.67 \mu\text{s}$ (i.e., 250-m range) intervals to the digital signal processor (DSP).

The RDA unit collects and monitors the status of a few hundred parameters (e.g., power supply voltages, environmental conditions, safety interlocks, etc.) and passes, at regular intervals, this information to the host computer, which determines the status of the system.

The proposed RDA computing platform is based on the American National Standard Institute's Verse Model Eurocard (VME)-64 chassis and equipment. VME is currently the most accepted and available bus architecture and will likely remain so for the foreseeable future. The host computer manages and performs task initiation, process scheduling, resource management, status monitoring and control, data transfer, etc.

At precise time intervals, the synchronizer generates the digital commands required for the transmission, reception, and processing of signals, as well as those required for the built-in-test equipment (BITE) and calibration circuitry. Tests and calibrations are performed at the end of every volume scan to maintain proper operation of the radar and accuracy of the processed data. Approximately 80 signals must be either accurately monitored or generated during every volume scan. About 60 more signals will be added if polarimetric capability is implemented.

The DSP subsystem performs prescaling, clutter filtering, and estimates spectral moments. The DSP consists of an array of processing elements connected through its own high-speed interlink and RACEway to accommodate the high data rates not available on the VME bus (Zahrai et al. 1998).

3. Antenna upgrades for polarimetric rainfall measurements

One of the enhancements to the WSR-88D is the addition of a polarimetric capability to improve rainfall estimation and to identify precipitation types (e.g., distinguish rain from hail, snow, etc.; Seliga and Bringi 1976, 1978; Balakrishnan and Zrnić 1990). Relations between radar reflectivity factor Z and rainfall rate R have been used for several decades to estimate rainfall accumulation, forecast flash flood conditions, etc. Although high reflectivity factor values correlate with high rainfall rates, there is no unique relation between the two.

Rainfall rate based upon Z constrains the assumed drop size distribution to one having a single parameter; in general the drop size distribution can only be described accurately by a function having many more parameters. On the other hand, Zawadzki (1984) points out that variability of drop size distributions is only one of many factors that affect the accuracy with which radar measures rain, and it is not necessarily the most important.

But Sachidananda and Zrnić (1986) demonstrate that the specific differential phase K_{DP} —the differential propagation phase shift per unit length between vertically, V, and horizontally, H, polarized waves—is proportional to the rainfall rate. Moreover, they show that K_{DP} is relatively insensitive to the form of the rain's drop size distribution. Furthermore, Zrnić and Ryzhkov (1996) have shown that the specific differential phase method of measuring rainfall rates overcomes many of the other factors (e.g., calibration errors; attenuation due to wet radome and rain along the propagation path; partial beam blockage; thresholds on reflectivity to eliminate hail bias, which causes underestimation of extreme rainfalls; ground clutter canceler bias; etc.) that limit rain measurement accuracy. Thus, the addition of a polarimetric capability to the WSR-88D should provide, for the first time, a revolutionary approach to the operational radar measurement of rainfall over the United States. The antenna is critical in developing a polarimetric sensing capability.

a. Three- versus four-spar feed support assembly

Early in planning modifications to the research WSR-88D radar for conversion to a polarimetric Doppler weather radar, consideration was given to change the three equally spaced feed supports (one in the vertical plane) to four with symmetry about the horizontal and vertical directions. This should match the radar antenna's radiation pattern for the H and V polarized waves; it has been shown that artifacts in differential reflectivity fields are related to the mismatch of sidelobes in high reflectivity gradient regions (Chandrasekar and Keeler 1993).

The blockage of secondary radiation by the spars creates a ridge of enhanced sidelobes in planes perpendicular to the spar's projection onto the aperture of the reflector. Thus, the three-spar support assembly generates three ridges of enhanced sidelobes, whereas the four-spar assembly generates only two ridges. Although the use of four spars spaced 90° apart reduces the number of ridges to two, the area of blocked illumination is doubled, and thus the sidelobe enhancement along the ridges should be 6 dB higher on average (Doviak et al. 1998).

Researchers at Colorado State University (CSU), National Center for Atmospheric Research (NCAR), and NSSL have opted for a four-spar feed support assembly for their polarimetric antennas. Since the CSU and NCAR reflector diameters are the same as that for the WSR-88D antenna, we should expect to see strong similarities in the radiation patterns; comparisons of patterns indicate this is indeed the case. But the measurements in planes passing through the enhanced ridges of sidelobes due to spar blockage show that the sidelobe levels of the CSU antenna exceed, by as much as 10 dB, the NEXRAD specifications and are significantly worse than that of the WSR-88D radiation pattern which

met these specifications before, and meets them, as well, after the change of feed to transmit H, V waves (Doviak et al. 1998). Therefore, the present three-spar configuration is preferred. The higher sidelobe levels of the CSU radar's radiation pattern is attributed to the larger size spars used to support the CSU feed.

b. Pattern measurements of the radiation fields from the R&D WSR-88D

Radiation pattern measurements of a number of newly fabricated WSR-88D antennas without radomes have been made by the manufacturer (i.e., Andrew Canada, Inc.) on their antenna range. Because radiation pattern measurements were not made for any WSR-88D antennas after assembly on site, nor with a fully assembled radome, it was imperative to make measurements for the KOUN, WSR-88D antenna before the feed was changed from a single port feed, designed to transmit H waves, to a feed with two ports, designed to transmit either or both H and V waves. The KOUN radiation patterns, measured at NSSL in 1997, before the change of feed, demonstrate that there are no significant changes in the performance of the antenna installed in 1988 from those tested by the manufacturer (Doviak et al. 1998).

After the change of feed, measurements were made of the patterns of radiation for H and V waves. The KOUN pattern for H waves is almost exactly that obtained with the original single-port WSR-88D feed (Doviak et al. 1998). In Fig. 2a, the KOUN's radiation pattern, with the new dual-port feed, is plotted for the H wave. The envelope of sidelobes, measured by Andrew Canada, Inc., for one of the WSR-88D antennas *without* a radome, is shown by the dashed lines in Fig. 2a. Note that sidelobe levels, on average, are larger. Comparisons of measurements of radiation patterns made by Andrew Canada, Inc. with and without a partially assembled radome suggested that a fully assembled radome could increase sidelobes as much as 1 or 2 dB. Thus, some of the increase over that measured without radome could be due to the radome.

The solid lines in Fig. 2a are the specified limits that sidelobe radiation with radome must not exceed. For sidelobe levels outside the $\pm 10^\circ$ interval, a sidelobe exceeding this limit is allowed, provided that integration with its two adjacent sidelobes does not exceed the limit (NEXRAD 1992, pp. 3–11). But the radiation pattern in Fig. 2a is in a plane on which sidelobes are enhanced because of scatter and blockage by the feed support strut, which lies in the vertical plane. Thus, the sidelobe levels plotted in Fig. 2a represent higher than average sidelobes.

The H and V patterns agree for the most part to a fraction of a decibel down to the -20 -dB level (Fig. 2b), but some of the differences could be due to measurement noise. For example, the first several sidelobes along the elevation scan agree better than those along the azimuth scan; this is because the main ra-

diation lobe in the elevation scan is directed well above the scatterers on the ground, whereas for the azimuth scan, the elevation angle is 0.5° , causing the lower edge of the main beam to illuminate objects on the ground. Thus, the sidelobes in the azimuth scan are likely subjected to interference from scatter of the main lobe illuminating ground objects (Doviak et al. 1998).

To minimize the influence of measurement noise, Gaussian functions fitted to the H, V radiation patterns were compared. The 3-dB widths of the fitted Gaussian patterns agree to within 0.03° , corresponding to a 0.1-dB difference of radiation at the -3 -dB levels. Differences between the data and the fitted Gaussian functions are as much as 0.4 dB in the range of normalized gains from 0 to -10 dB; most likely, these differences are errors in the measurements and are not representative of the true departures of the gain. Pattern measurements on a well-designed range are needed to better quantify these small differences in the H, V radiation patterns.

Cross-polarization patterns were also recorded. The H and V cross-polarization patterns are remarkably similar, although the vertical cross-polar signals appear to be a few decibels higher in certain directions, and again, this could be due to limitations of our antenna range (e.g., terrain scatter; Doviak et al. 1998). The peaks of cross-polar radiation from the H and V ports were found to lie along the axis of the main lobe. The H port cross-polar radiation pattern is plotted in Fig. 2c; the peak in the cross-polar pattern for the V port is about 5 dB higher.

Because the peak of cross-polar radiation is observed along the main lobe axis, whereas a null of cross-polar radiation is expected along the principal planes (i.e., along the azimuth and elevation scans through the main lobe axis; Fradin 1961), the peak in cross-polar radiation might be related to incorrect angular orientation of the feed about the focal axis. This would cause simultaneous transmission of strong H (or V) and weak V (or H) polarized waves. To determine if angular orientation of the feed was responsible for this peak, and to minimize the effects of cross-polar coupling due to terrain scatter, we made measurements with a standard gain horn atop the (KCRI) tower located about 300 m from the KOUN tower. The KCRI is the WSR-88D in use by the NWS's Operational Support Facility, OSF. This location places the radiation source in the near field of the antenna where the radar beam is still collimated (i.e., it is essentially cylindrical in shape), but the angle to the terrain is several degrees below the beam axis. With the main beam axis pointed at the standard gain horn, we rotated the horn until a cross-polar null was established, and this rotation angle was recorded. With either the H or V ports connected to the receiver, the tilt is zero within the accuracy of measurement (i.e., about $\pm 0.1^\circ$). Thus, it is concluded that the on-axis cross-polar peak is due to cross-polar

radiation from the dual-port feed. Pattern measurements for the dual-port feed support this conclusion (Doviak et al. 1998). Nevertheless, the cross-polar levels meet NEXRAD specifications and are sufficiently low that they should not compromise measurement of the polarimetric parameters.

4. Selection of the polarimetric basis and implementation

The selection of a polarimetric basis should be founded on scattering theory and the physical properties of the hydrometeors. For example, it does little good to select a basis for purely engineering reasons, as was the case for the first ten WSR-88D radars. For these 10 radars, Right Hand Circular (RHC) or Left Hand Circular (LHC) polarization was chosen for transmission, and LHC or RHC (i.e., the cross-polar or main channel signal) was chosen for reception to reduce losses within the radar by eliminating the need for a circulator. This would have been a good engineering choice if hydrometeors were spherical, but since most are not, there was significant loss of echo power due to the conversion of the copolar wave to the cross-polar one as the waves propagate through rain containing aspherical drops (Doviak and Zrnić 1993, section 8.5.2.3).

The purpose of selecting a polarimetric basis, different than the single linear polarimetric state of horizontally polarized waves used in the current WSR-88D radars, is to retrieve additional and/or better information about the type and quantity of precipitation. Therefore, the selected polarimetric basis should be one that can provide the most accurate information about precipitation without degrading the existing capabilities of the WSR-88D, while constraining the cost of implementation and maintenance to an affordable amount.

At long wavelengths (e.g., 10 cm), a good approximation to the shape of most hydrometeors is the oblate/prolate spheroid. Thus, there are only a few physical properties of the hydrometeors that can influence the magnitude, phase, and polarization state of the backscattered signals. These properties are:

- 1) electrical size $\tilde{\sigma}$ (for spherical drops $4\pi\tilde{\sigma} = \sigma_b$, the backscattering cross section), which is a function of the hydrometeor's complex susceptibilities (or polarizabilities) p_a, p_b (see Doviak and Zrnić 1993, section 8.5.2.4 for definition; note that a, b replaces v, h in their equations; other corrections can be found online at www.nssl.noaa.gov/papers/books.html) along its minor "a" or its major "b" axes;
- 2) apparent canting angle ψ (i.e., the orientation of the hydrometeor's axis of symmetry projected onto the plane of polarization);
- 3) dispersion of the apparent canting angles (i.e., hy-

- drometeors usually wobble and vibrate as they respond to turbulent forces and shear); and
- 4) ellipticity or shape, which is related to a shape parameter $v = (p_b - p_a)/(p_b + p_a)$, which can be derived from McCormick and Hendry (1975).

a. The polarimetric bases selection in absence of propagation effects

If there is no precipitation in the intervening media between the radar and the scattering volume, the circular polarization basis provides relatively simple relations between the cited properties and the elements, $\langle s_{ij}s_{kl}^* \rangle$, of the backscattering covariance matrix \mathbf{Co} for the sampled resolution volume (McCormick and Hendry 1975; Ryzhkov 1993). For example, 1) if scatterers are spherical, $\tilde{\sigma} = \langle |s_{rr}|^2 \rangle$; 2) the size-weighted shape $\langle \tilde{\sigma}|v|^2 \rangle = \langle |s_{rr}|^2 \rangle$, where the shape parameter v for water drops is nearly 0 if they are small (i.e., if they are spherical), 0.25 if they are large (i.e., 6-mm diameter at which they have an oblate spheroidal shape), and 1.0 if the scatterers are strongly oblate; and 3) the mean canting angle $\langle \psi \rangle$ is directly obtainable from $-4\langle \psi \rangle = \arg \langle s_{rr}s_{rl}^* \rangle - \arg \langle s_{ll}s_{rl}^* \rangle$. The indices are r (RHC) or l (LHC) for the circular polarization basis and h or v for the H, V linear basis, respectively; the first and second indices refer to the received and transmitted polarizations. The angle brackets denote an ensemble average of the hydrometeor's properties (e.g., equivolume diameter D_e , canting angle ψ , etc.); that is,

$$\langle s_{ij}s_{kl}^* \rangle = \int P(\mathbf{X})s_{ij}s_{kl}^* d\mathbf{X}, \quad (1)$$

where $P(\mathbf{X})$ is the probability density of the scatterer's properties \mathbf{X} .

Although the backscattering matrix elements in the linear basis have a more complicated relation with the hydrometeor's properties (because mean shape and mean canting angle cannot be separated) than that found with the circular basis (Doviak et al. 1998), propagation effects and other practical considerations discussed in the next sections offset this disadvantage.

b. The polarimetric basis selection in the presence of propagation effects

Because most hydrometeors have an axis of symmetry near vertical, H or V linearly polarized waves practically remain in the same pure polarization state as they propagate through rain. (That is, a pure horizontally transmitted wave retains this polarization.) In contrast, circularly polarized waves depolarize, generally to a polarized elliptical state, as they propagate through rain, and propagation effects must be considered to obtain the elements of \mathbf{Co} . Although there is no depolarization of H and V waves propagating through precipitation (if the hydrometeors' axes of symmetry are vertical), there

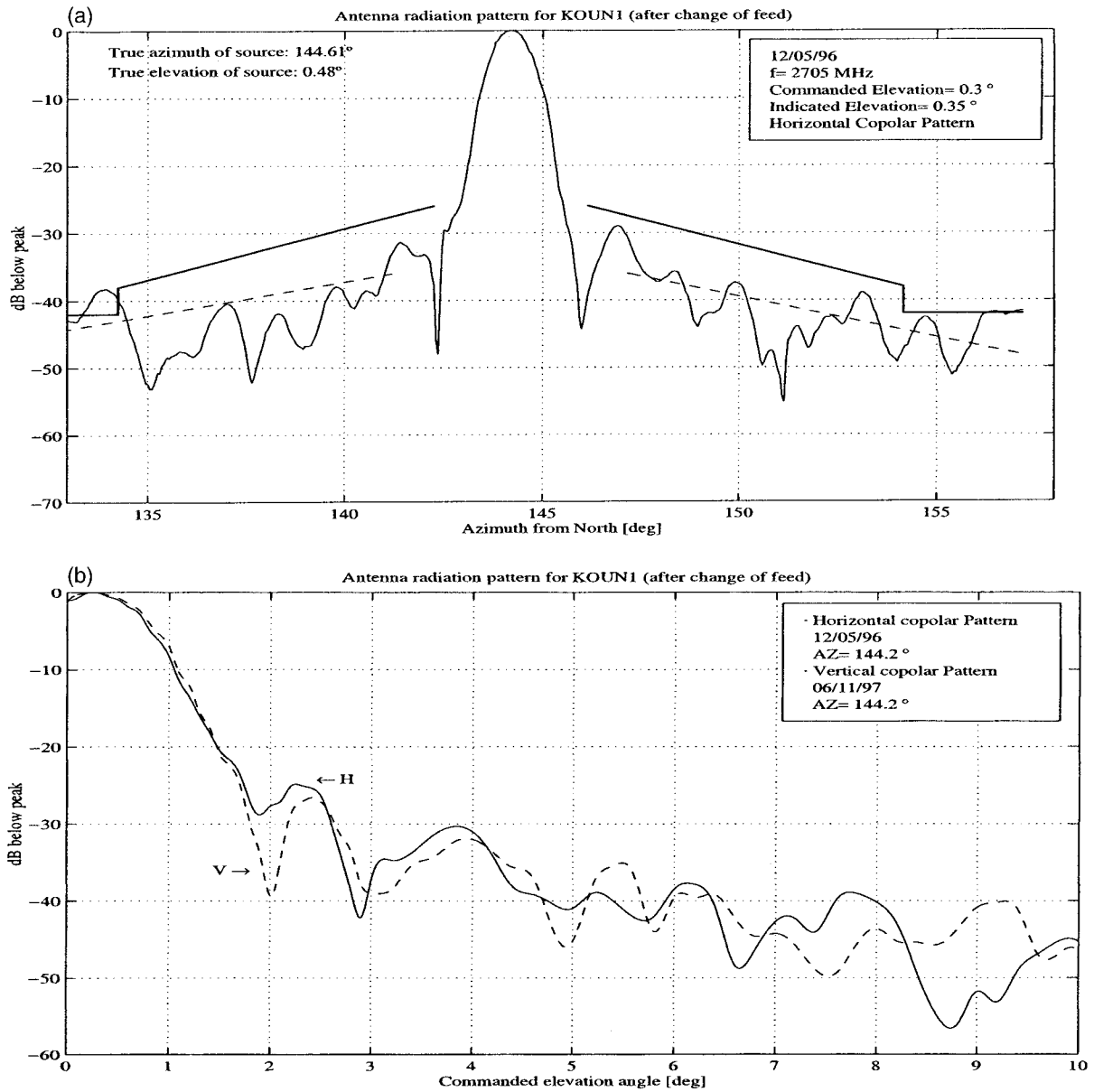


FIG. 2. (a) The R&D WSR-88D copolar pattern of horizontally polarized radiation at a frequency of 2705 MHz. The solid lines are the specified limits for sidelobes; the dashed lines are the estimated sidelobe envelopes of a newly fabricated WSR-88D antenna without its radome. (b) A comparison of the copolar radiation patterns for H and V radiation as a function of elevation angle.

could be differential attenuation and differential phase shift between the two waves. Nevertheless, the H, V components of the wave propagate independently. For weather radars operating at long wavelengths, attenuation is usually negligible. This permits direct measurement of \mathbf{Co} for the sampled resolution volume V_6 (Doviak et al. 1998, sections 4.4.4 and 7.8), whereas measurements require extensive corrections if circularly polarized echoes are received. The elements of the back-scattering covariance matrix \mathbf{Co} for the hydrometeors within the sampled V_6 are, for the most part, the ones

sought after by radar meteorologists. One exception is the specific differential phase, which is a function of the forward scattering properties of the propagation medium.

The specific differential phase K_{DP} , derived from the elements of the transmission matrix \mathbf{T} , can be used to estimate rainfall without the need to calibrate the radar (Doviak and Zrnić 1993, section 8.4.3). Because canting angles ψ are believed to be narrowly distributed about a mean near zero (Jameson 1983; Beard and Jameson 1983), \mathbf{T} reduces to

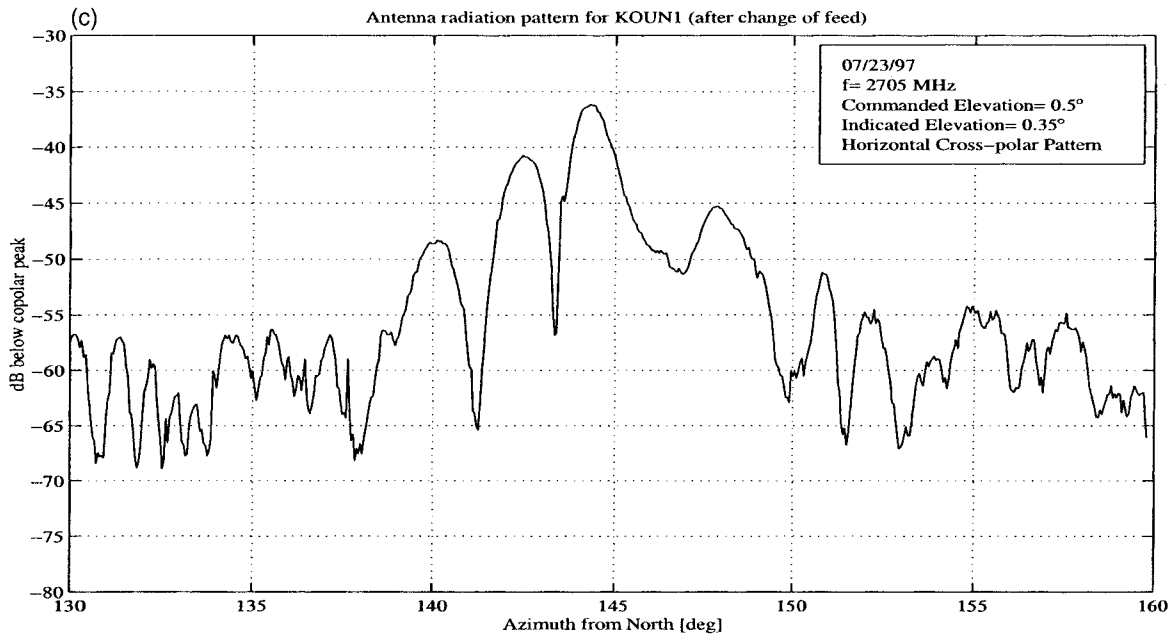


FIG. 2. (Continued) (c) The cross-polar pattern for the H port of the dual-port feed. The standard gain horn is oriented to transmit vertically polarized waves, and the WSR-88D receives H waves.

$$\mathbf{T} = \begin{bmatrix} T_h & 0 \\ 0 & T_v \end{bmatrix}, \quad (2)$$

in which the matrix elements,

$$T_h = \ell_{hv}^{-1/2} \exp\left[-j\frac{\phi_{DP}}{2}(1 - \sigma_\psi^2)\right] \quad \text{and}$$

$$T_v = \exp\left(-j\sigma_\psi^2\frac{\phi_{DP}}{2}\right), \quad (3)$$

are obtained from more general formulas of Oguchi (1983). The propagation differential phase $\phi_{DP} = \phi_{vv} - \phi_{hh}$ is the round-trip phase difference between the phases ϕ_{vv} and ϕ_{hh} of the received V and H waves in absence of canting angle dispersion σ_ψ (the rms dispersion of canting angles). Here, ℓ_{hv} ($\ell_{hv} \geq 1$) is the one-way differential power loss for the horizontal component.

The transformation matrix $\mathbf{V}^{(\epsilon)}$ of measurands relates the components of the transmitted electric field vector $[E_h \ E_v]$ at the radar to those components returned by a scatterer. The elements of $\mathbf{V}^{(\epsilon)}$ are proportional to the voltages measured in the H, V receivers if $E_h = E_v$, and the components of the electric field are applied one at a time (e.g., V_{hv} is proportional to the voltage in the H channel if only V polarized waves are transmitted). Thus,

$$\mathbf{V}^{(\epsilon)} \equiv \begin{bmatrix} V_{hh} & V_{hv} \\ V_{hv} & V_{vv} \end{bmatrix} = \begin{bmatrix} T_h & 0 \\ 0 & T_v \end{bmatrix} \begin{bmatrix} s_{hh} & s_{hv} \\ s_{vh} & s_{vv} \end{bmatrix} \begin{bmatrix} T_h & 0 \\ 0 & T_v \end{bmatrix}$$

$$= \mathbf{T}'\mathbf{S}\mathbf{T}, \quad (4)$$

where the superscript t denotes a transposed matrix or vector and $S_{hv} \equiv S_{vh}$. In the balance of this section, it is assumed that H, V waves are alternately transmitted but simultaneously received.

The expected differential reflectivity factor $\langle \hat{Z}_{dr} \rangle$ ($\langle \cdot \rangle$ denotes the expected value of an estimate \hat{Z}_{dr}), calculated from the elements of $\mathbf{V}^{(\epsilon)}$ is

$$\langle \hat{Z}_{dr} \rangle \equiv \frac{\langle |\hat{V}_{hh}|^2 \rangle}{\langle |\hat{V}_{vv}|^2 \rangle} = \frac{|T_h|^4 \langle |s_{hh}|^2 \rangle}{|T_v|^4 \langle |s_{vv}|^2 \rangle} = \frac{1}{\ell_{hv}^2} Z_{dr}, \quad (5)$$

where Z_{dr} is the intrinsic differential reflectivity factor (i.e., the Z_{dr} of the sampled V_0). Equation (5) indicates that $\langle \hat{Z}_{dr} \rangle$ is biased by the square of the differential transmission loss. (The square arises because there is a two-way loss.) In stratified rain at long wavelengths, the attenuation is usually negligible, and $\langle \hat{Z}_{dr} \rangle$ is a very good estimate of Z_{dr} . In convective storms and along squall lines, however, the differential transmission loss can be significant and needs to be known. It is possible to estimate the total attenuation and the differential attenuation by means of the propagation differential phase ϕ_{DP} (Balakrishnan and Zrnić 1989; Bringi et al. 1990; Ryzhkov and Zrnić 1995).

Likewise, the expectation of the linear depolarization ratio estimates $\hat{\text{Ldr}}_{vh}$ (Doviak and Zrnić 1993, p. 242),

$$\langle \hat{\text{Ldr}}_{vh} \rangle \equiv \frac{\langle |\hat{V}_{vh}|^2 \rangle}{\langle |\hat{V}_{hh}|^2 \rangle} = \frac{|T_v|^2 \langle |s_{hv}|^2 \rangle}{|T_h|^2 \langle |s_{hh}|^2 \rangle} = \ell_{hv} \text{Ldr}_{vh}, \quad (6)$$

is a biased estimate of the intrinsic Ldr_{vh} . [The lower case “dr” is used to denote the ratio directly, whereas the upper case “DR” (e.g., LDR_{hv}) will be used to express the ratio in decibels.]

The last important linear polarimetric parameter is the correlation coefficient $\rho_{hv}(0)$ of the two received copolar signals calculated at zero lag from the elements of $\mathbf{V}^{(c)}$. If we ignore the usually small effects of depolarization upon backscatter discussed in section 5c(2) the expected value of the measured correlation coefficient is

$$\begin{aligned} \langle \hat{\rho}_{hv}(0) \rangle &\equiv \frac{\langle \hat{V}_{hh} \hat{V}_{vv}^* \rangle}{\sqrt{\langle |\hat{V}_{hh}|^2 \rangle \langle |\hat{V}_{vv}|^2 \rangle}} \\ &= \frac{\langle s_{hh} s_{vv}^* \rangle}{\sqrt{\langle |s_{hh}|^2 \rangle \langle |s_{vv}|^2 \rangle}} \\ &\quad \times \exp[j\phi_{\text{DP}}(1 - 2\sigma_\psi^2) - j(\delta_{vv} - \delta_{hh})], \quad (7) \end{aligned}$$

in which $\delta_\ell = \delta_{vv} - \delta_{hh}$ (usually very small at wavelengths greater than 10 cm) is the intrinsic differential phase shift between H and V waves produced upon backscatter from nonspherical scatterers in V_6 . If H and V waves are alternately transmitted, as assumed in this section, $\hat{\rho}_{hv}(0)$ needs to be calculated from H, V signals obtained from alternate time-lag-separated samples (Doviak and Zrnić 1993, section 6.8.5). Whereas the magnitude of $\hat{\rho}_{hv}(0)$ is an unbiased estimate of the intrinsic copolar correlation coefficient magnitude $|\rho_{hv}(0)|$ of the H, V signals upon backscatter from V_6 (if the mean canting angle is zero), the argument of $\hat{\rho}_{hv}(0)$ as an estimate for δ_ℓ is biased by $\phi_{\text{DP}}(1 - 2\sigma_\psi^2)$. Because ϕ_{DP} is typically larger than δ_ℓ , it strongly biases the δ_ℓ estimates, which cannot be separated in the measurement.

On the other hand, because ϕ_{DP} is uniquely related to rainfall rate, it is not considered to be a biasing nuisance. Quite the contrary, ϕ_{DP} is sought after to improve rainfall estimates. But, as seen from (7), using the argument of $\hat{\rho}_{hv}(0)$ as an estimate of ϕ_{DP} {i.e., $\hat{\phi}_{\text{DP}} = \arg[\hat{\rho}_{hv}(0)]$ } incurs biases due to σ_ψ and δ_ℓ . Interestingly, the argument of $\langle \hat{\rho}_{hv}(0) \rangle$ is principally related to the propagation differential phase shift due to aspherical scatterers in the medium *between* the radar and the resolution volume V_6 , whereas the magnitude of $\langle \hat{\rho}_{hv}(0) \rangle$ is principally related to the properties of the scatterers *within* V_6 .

c. The circular polarimetric basis in presence of propagation effects

The transformation of a vector, from an expression in a linear basis to one in a circular basis, is given by

$$\mathbf{E}_c = \mathbf{C}\mathbf{E}_\ell, \quad (8)$$

where \mathbf{E}_c is defined as the column vector $[E_r \ E_\ell]^t$ of the circularly polarized electric field, \mathbf{E}_ℓ is the column vector $[E_h \ E_v]^t$ for linear polarized waves, and \mathbf{C} is

$$\mathbf{C} \equiv \frac{1}{\sqrt{2}} \begin{bmatrix} 1 & j \\ 1 & -j \end{bmatrix}. \quad (9)$$

These definitions, and the convention $e^{j\omega t}$ for harmonic waves, are consistent with accepted standards (IEEE 1983). That is, if $[E_h \ E_v]$ constitute the axes of a right-handed coordinate system $[y \ x]$, propagation is in the direction of z (e.g., Bringi and Hendry 1990, their Fig. 2.1).

We can use the matrix \mathbf{C} to convert the incident circular polarimetric basis to a linear one (i.e., $\mathbf{E}_\ell = \mathbf{C}^{-1}\mathbf{E}_c$; Doviak and Zrnić 1993, section 8.5.2.1) so that we can directly use the elements of the matrices for backscatter \mathbf{S} and transmission \mathbf{T} already specified for the linear basis. Thus, the transformation matrix $\mathbf{V}^{(c)}$ for circularly polarized waves is

$$\mathbf{V}^{(c)} \equiv \begin{bmatrix} V_{rr} & V_{lr} \\ V_{rl} & V_{ll} \end{bmatrix} = \mathbf{C}^* \mathbf{T}^t \mathbf{S} \mathbf{C}^{-1}, \quad (10)$$

from which we find that

$$V_{rr} = \frac{1}{2}(T_h^2 s_{hh} - 2jT_h T_v s_{hv} - T_v^2 s_{vv}), \quad \text{copolar,}$$

$$V_{lr} = V_{rl} = \frac{1}{2}(T_h^2 s_{hh} + T_v^2 s_{vv}), \quad \text{cross-polar,}$$

and

$$V_{ll} = \frac{1}{2}(T_h^2 s_{hh} + 2jT_h T_v s_{hv} - T_v^2 s_{vv}), \quad \text{copolar.} \quad (11)$$

For sufficiently short propagation paths in rain, magnitudes of V_{rr} and V_{ll} are relatively small compared to the magnitude of V_{lr} because nearly all the power backscattered from rain is in the cross-polarized wave (if each scatterer is circularly symmetric about the direction of propagation all the power is in the cross-polar wave) and because the right and left handedness of the wave is defined with respect to an observer looking in the direction of propagation for *both* the incident and the backscattered waves.

From the elements of the transformation matrix $\mathbf{V}^{(c)}$, one can calculate the various covariance terms associated with the simultaneous reception of the two circularly polarized components alternately transmitted. Much of the early effort in utilizing the matrix elements in (11), which includes the effects of propagation, focused on estimating *backscattering* parameters (e.g., the reflectivity factor, depolarization ratio, etc.) of the sampled V_6 . Useful estimation required corrections for the effects of propagation (Jameson and Davé 1988; Bebbington et al. 1987).

The focus on the backscattering parameters was expanded to include those from the transmission matrix \mathbf{T} after Sachidananda and Zrnić (1986) showed that rainfall rate estimated from the single parameter K_{DP} (i.e., the range rate of ϕ_{DP} change) is relatively insensitive to drop size distributions, and that K_{DP} offers many other advantages. Because important meteorological variables (e.g., rainfall rate, precipitation type, etc.) are usually derived from terms in the covariance matrix \mathbf{Co} , as well

as terms in the transmission matrix \mathbf{T} (e.g., differential phase ϕ_{DP}) associated with the linear polarimetric basis, the procedure to estimate precipitation parameters then shifted to extracting the linear basis terms from the components of $\mathbf{V}^{(c)}$ (e.g., McGuinness et al. 1987; Holt 1988).

Because K_{DP} and the differential reflectivity Z_{DR} have many robust properties for the measurement of rainfall (Ryzhkov and Zrnić 1996; Zrnić and Ryzhkov 1996), we shall focus our attention on the extraction of ϕ_{DP} and Z_{DR} from the elements of $\mathbf{V}^{(c)}$. Torlaschi and Holt (1993) showed that, under the condition that all drops are equioriented with a vertical axis of symmetry, ϕ_{DP} is related to the circular basis covariance elements by

$$\arg\left\{\frac{\langle|\hat{V}_{lr}|^2\rangle - \langle|\hat{V}_{rr}|^2\rangle}{2} - j\text{Im}[\langle\hat{V}_{rr}\hat{V}_{lr}^*\rangle]\right\} = \phi_{DP} + \delta_\ell, \quad (12)$$

where δ_ℓ ,

$$\delta_\ell = \arg\left\{\frac{\langle|s_{lr}|^2\rangle - \langle|s_{rr}|^2\rangle}{2} - j\text{Im}[\langle s_{rr}s_{lr}^*\rangle]\right\} = \arg\{s_{vv}s_{hh}^*\}, \quad (13)$$

is the differential phase shift upon backscatter in the linear basis.¹ If scatter is from rain at a 10-cm wavelength, $\delta_\ell \approx 0$ (Torlaschi and Holt 1993). Under this condition, using nonswitched (e.g., only RHC waves are transmitted) circularly polarized transmitted waves and calculation of the covariance elements for the two received circularly polarized waves, the argument in Eq. (12) should give a relatively unbiased estimate of propagation differential phase ϕ_{DP} .

On the other hand, if drops have a nonzero mean and/or dispersion of canting, the argument of (13) contains an additional term proportional to $\langle|s_{hv}|\rangle$ (Doviak et al. 1998), which can be obtained by substituting the matrix elements (11) into (12). Although drops within the sampled V_6 likely have, on average, a zero canting angle, canting angle dispersion causes s_{hv} to differ from zero. Nevertheless, for rain within the sampled V_6 , this term remains negligible. But, if the scattering volume is filled with a mixture of rain and hail, omission of this term leads to significant (i.e., up to 10%) biases in rainfall estimates.

Torlaschi and Holt (1993) also relate the differential reflectivity to the elements of the transformation matrix:

$$Z_{DR} = 10 \log \frac{\langle|\hat{V}_{lr}|^2\rangle + \langle|\hat{V}_{rr}|^2\rangle + 2\text{Re}(\langle\hat{V}_{rr}\hat{V}_{lr}^*\rangle)}{\langle|\hat{V}_{lr}|^2\rangle + \langle|\hat{V}_{rr}|^2\rangle - 2\text{Re}(\langle\hat{V}_{rr}\hat{V}_{lr}^*\rangle)} + \ell_{hv}^2. \quad (14)$$

As before, to be consistent with our definitions and convention, the signs multiplying the real parts of (14) have been changed from that used by Torlaschi and Holt. The differential attenuation ℓ_{hv} in rain can be estimated from measurements of ϕ_{DP} , as noted in section 4b.

d. Comparisons of linear and circular polarimetric bases

Examining (12) and (14), it is apparent that computations of ϕ_{DP} and Z_{DR} both involve three covariance terms ($\langle|\hat{V}_{lr}|^2\rangle$, $\langle|\hat{V}_{rr}|^2\rangle$, and $\langle\hat{V}_{rr}\hat{V}_{lr}^*\rangle$, even if $\ell_{hv} = 0$), whereas a similar computation in a linear basis involves one for ϕ_{DP} and two for Z_{DR} . A smaller number of terms usually leads to a smaller estimate variance which, in turn, should lead to smaller variance in rainfall estimates. Because most hydrometeors in rain are nearly spherical, an obvious limitation of the circular basis is that the covariance terms, with the exception of $\langle|\hat{V}_{lr}|^2\rangle$, are typically weak. Thus, in general, hydrometeor information will be strongly corrupted by receiver noise except in regions of very strong reflectivity. For example, Barge (1970) was able to extract $\langle|s_{rr}|^2\rangle$ data only in regions where reflectivity factor was larger than 45 dBZ. In conclusion, polarimetric parameters (e.g., specific differential phase K_{DP} and differential reflectivity Z_{DR}), robustly related to rainfall measurements in many rainfall regions, cannot be reliably retrieved, as also found by English et al. (1991), from measurements in the circular basis.

Furthermore, because circularly polarized waves are converted from one sense to another when propagating through rain, there could be severe underestimates of reflectivity (e.g., Fig. 8.12 of Doviak and Zrnić 1993) if only the cross-polar channel (i.e., the usually stronger main channel) is used to estimate reflectivity. Assuming H, V waves are alternately transmitted and received, the expected measured reflectivity factor $\langle\hat{Z}_c\rangle$ for circularly polarized waves, normalized to the expected measured reflectivity factor $\langle\hat{Z}_h\rangle$ for horizontally polarized waves, is

$$\frac{\langle\hat{Z}_c\rangle}{\langle\hat{Z}_h\rangle} \equiv \frac{\langle|\hat{V}_{lr}|^2\rangle}{\langle|\hat{V}_{hh}|^2\rangle} = \frac{1}{4}[1 + A + B], \quad (15a)$$

where

$$A \equiv \frac{\ell_{hv}^2}{Z_{dr}}, \quad B \equiv \frac{2\ell_{hv}|\rho_{hv}(0)|}{\sqrt{Z_{dr}}} \cos[\phi_{DP}(1 - 2\sigma_\psi^2)]. \quad (15b)$$

Equation (15a), in decibels, is plotted in Fig. 3 as a function of the differential phase ϕ_{DP} , assuming $Z_{DR} = 2$ dB (the uppercase subscripts denote decibels), $|\rho_{hv}(0)| = 0.98$, $\ell_{hv} = 1$, and $\sigma_\psi^2 = 0$. Even in absence of propagation effects (i.e., at $\phi_{DP} = 0$), there is a 1-dB difference in the two reflectivity factors because of the cross coupling of circular polarized waves in V_6 . It is quite apparent that if ϕ_{DP} is larger than about 20° (e.g., corresponding to 10 km of propagation in a 40 mm h⁻¹ rainfall rate), the bias in Z_c is significant (i.e., >1 dB),

¹ To be consistent with our definitions and convention, $-j$ is used in (12) and (13) in place of $+j$ used by Torlaschi and Holt.

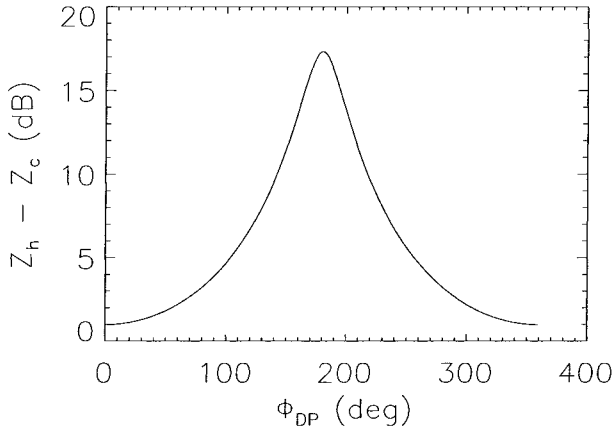


FIG. 3. The expected difference $\langle Z_h \rangle - \langle Z_c \rangle$ in reflectivity factors measured (in dB) with linearly and circularly polarized waves vs ϕ_{DP} . Canting angle dispersion and differential attenuation are assumed to be negligibly small. Here, $Z_{DR} = 2$ dB and $|\rho_{hv}(0)| = 0.98$ are the intrinsic values in the sampled V_6 .

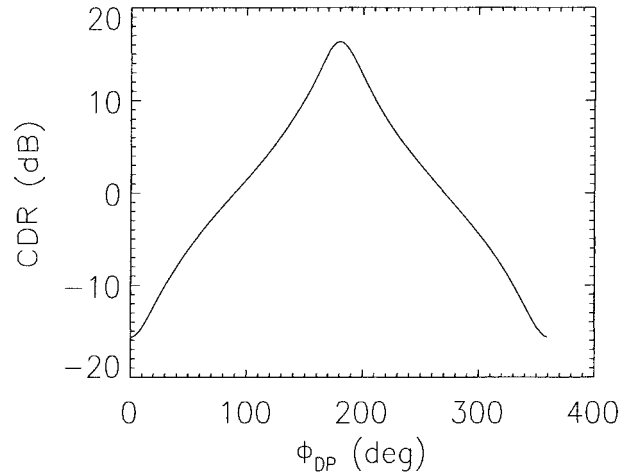


FIG. 4. The expected measured circular depolarization ratio $\langle CDR \rangle$ (in dB) vs ϕ_{DP} . The intrinsic CDR value is that for $\phi_{DP} = 0$. Parameter values are the same as in Fig. 3, and $LDR_{vh} = -25$ dB.

and for $\phi_{DP} > 50^\circ$, it is unacceptable. Torlaschi and Pettigrew (1990) showed that for observations of convective storms with circularly polarized transmissions, propagation effects at a 10-cm wavelength can lead to an underestimation of the reflectivity factor by an amount that is of the same order of magnitude as the attenuation at 5-cm wavelengths.

The intrinsic circular depolarization ratio (Cdr), defined as

$$\text{Cdr} \equiv \frac{\langle |s_{rr}|^2 \rangle}{\langle |s_{lr}|^2 \rangle}, \quad (16)$$

is invariant to the orientation of the hydrometeor's symmetry axis, unlike the linear depolarization ratio. Thus, *in absence of propagation effects*, the Cdr is directly measured, and it is useful in quantifying the ellipticity of nonspherical hydrometeors. For example, Barge (1974), using size spectra of rain from various geographical regions, showed that for the same reflectivity factor, tropical rain had CDR values several decibels lower than other types of rain. This simulated result suggests that tropical rain has a relatively high abundance of small drops, which are nearly spherical.

On the other hand, *in the presence of precipitation along the propagation path*, the expected measured Cdr has a dependence on differential propagation phase given by

$$\langle \text{Cdr} \rangle \equiv \frac{\langle |\hat{V}_{rr}|^2 \rangle}{\langle |\hat{V}_{lr}|^2 \rangle} = \frac{1 + A - B + 4\ell_{hv}Ldr_{vh}}{1 + A + B}. \quad (17)$$

This equation, in decibels, is plotted in Fig. 4 for the same parameters as those used to plot Fig. 3, and LDR_{vh} is assumed to be -25 dB. Figure 4 demonstrates the significance that propagation effects have on the measurement of Cdr. Thus, measurements with a circular polarization basis require correction for propagation effects (Bebbington et al. 1987). Cdr can also be computed

from measurements in the linear basis using (11). This estimate, however, would likely have a larger variance because it is indirectly derived.

As a last example of the biases introduced by the anisotropic propagation medium, consider McCormick and Hendry's (1975) method whereby the canting angle dispersion can be derived from $\text{ORTT} \equiv |s_{rr}s_{lr}^*| / [(\langle |s_{rr}|^2 \rangle \langle |s_{lr}|^2 \rangle)^{1/2}]$, the copolar to cross-polar correlation coefficient in the circular basis. But if we use this algorithm with parameters estimated in presence of precipitation along the propagation path, the circular backscattering matrix terms in ORTT must be replaced by the elements of the $\mathbf{V}^{(c)}$ (e.g., V_{rr} in place of s_{rr} , etc). Thus, the expected measured ORTT is

$$\begin{aligned} \langle \text{ORTT} \rangle &\approx \frac{|\langle \hat{V}_{rr} \hat{V}_{lr}^* \rangle|}{\langle |\hat{V}_{rr}|^2 \rangle^{1/2} \langle |\hat{V}_{lr}|^2 \rangle^{1/2}} \\ &= \frac{\left| 1 - A + j \frac{2\ell_{hv}|\rho_{hv}(0)|}{\sqrt{Z_{dr}}} \sin[\phi_{DP}(1 - 2\sigma_\psi^2)] \right|}{(1 + A + B)^{1/2} (1 + A - B + 4\ell_{hv}Ldr_{vh})^{1/2}}, \end{aligned} \quad (18)$$

from which we can deduce the effects of the propagation medium. This equation is plotted in Fig. 5 for the same parameters used in Fig. 3. Figure 5 indicates that propagation effects can significantly bias ORTT , and corrections are necessary if ORTT is used to estimate the intrinsic canting angle dispersion within the sampled V_6 .

In conclusion, although the circular polarization basis can, in principle, provide estimates of K_{DP} without switching the transmitted polarization, the estimation of this parameter would inevitably cause problems in the estimation of rainfall rate in weaker showers. But with circular polarization, the cross-polar signal does not depend on the orientation of hydrometeors; furthermore, in combination with the copolar signal, it leads to the

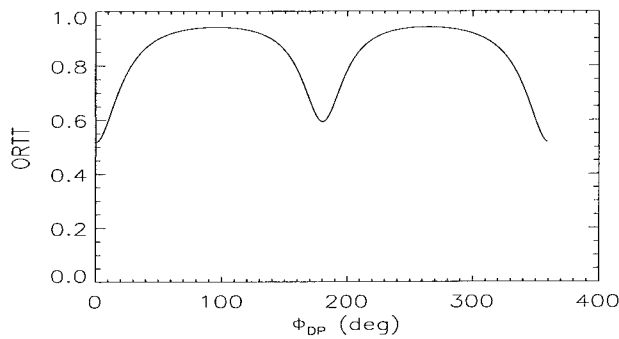


FIG. 5. The expected measured circular basis's correlation coefficient (ORTT) vs ϕ_{DP} . The intrinsic ORTT value is that for $\phi_{DP} = 0$. Parameter values are the same as in Fig. 3.

measurement of the mean apparent canting angle. Despite this advantage of the circular polarization basis, linear polarization offers simpler, more direct, and accurate quantitative measurements of rainfall without the need for extensive corrections. Furthermore, the H, V signals can be used to estimate (though likely with larger variance) the typically less needed CDR and ORTT parameters. Therefore, our choice rests with the linear H, V basis.

e. Methods of implementing the linear polarization basis

Several options exist for implementing the linear polarization basis, two of which were first suggested by Seliga and Bringi (1976), which involved (i) switching the transmitted polarization between H and V on a pulse-by-pulse basis and using a single receiver, and (ii) simultaneous transmissions of H and V with simultaneous reception using dual receivers. The microwave circuits in the KOUN can be configured to test the most promising polarimetric schemes. Scientists at NSSL, NCAR, and CSU have experience with alternately transmitting H, V polarizations wherein a high-power ferrite switch and a single receiver are used. This arrangement has possible operational deficiencies (discussed below) that prompted other approaches.

NCAR has implemented, in their S-Pol polarimetric radar, a high-speed rotary switch to alternately transmit H, V polarized waves and to simultaneously receive H, V echoes in a pair of receivers (Randall et al. 1997). A principal advantage of the mechanical switch is its excellent isolation (i.e., ≈ 50 dB) between H, V ports. Three disadvantages of this arrangement are its 1) relatively short lifetime, 2) excessive acoustic noise generated by the switch, and 3) unsuitability for the batch mode transmission (Doviak and Zrnić 1993) presently used with the WSR-88D, or the staggered or variable PRF transmissions, which are being considered for possible upgrades to the WSR-88D to mitigate the range-velocity ambiguity problem (Sachidananda et al. 1997, 1998).

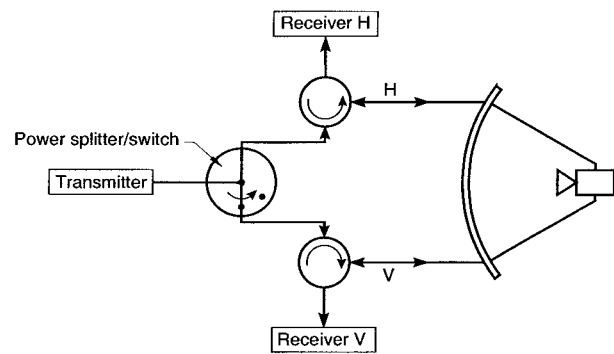


FIG. 6. A simplified block diagram illustrating the option of NSSL's R&D WSR-88D to switch from simultaneous transmission and reception of H, V waves to transmission and reception of horizontally polarized waves (i.e., the WSR-88D operational mode).

CSU has two transmitters, alternately pulsed at one-half the pulse repetition frequency of a single transmitter, to excite the H and V ports of the antenna. This approach achieves excellent isolation between the H and V signal paths and adds redundancy to the transmitter chain, but the cost of this system is high. A transfer switch in the two-channel receiving chain directs the strong H, V copolar signals into one receiver and the weaker cross-polar signal into another receiver (Brunkow et al. 1997). CSU has also tried simultaneous transmission of H and V polarizations with switched reception (i.e., a single receiver is alternately used) and with simultaneous reception using two receivers. Preliminary assessments of simultaneous versus alternate transmission and reception are given in sections 4f and 6.

NSSL is proposing simultaneous transmission and reception of the H, V polarizations. The schematic in Fig. 6 illustrates the basics of the system. Two modes of operation are planned: 1) a dual-polarization mode (power splitter/switch connected to the H and V channels), and 2) a single-polarization mode (power splitter/switch disconnected from the V channel). The single-polarization (H) mode is needed to test other potential improvements for the existing network of WSR-88Ds. Simultaneous transmission and alternate reception with a single receiver will also be tested. If needed, the proposed configuration could accommodate a high-power ferrite switch.

f. Relative merits of simultaneous versus alternate transmissions of H, V waves

We now contrast the benefits that are obtained using simultaneous transmission/reception with those obtained using alternate transmission/reception of H, V waves. Note, however, that simultaneous transmission/reception measurements are not performed in an orthogonal basis; that is, the received signals are not copolar and cross-polar to that transmitted. For example, the simultaneous transmission of H, V waves of equal

amplitudes will generate, in general, a right- or left-handed elliptically polarized wave having a $\pm 45^\circ$ tilt, but the pair of received signals will always be the H, V components, which can neither be copolar nor cross-polar to the transmitted wave. What is measured are the elements of the 2×2 coherency matrix of the scattered wave (two power terms and one complex correlation). It follows that unless the transmission and scattering matrices are diagonal in the linear H, V basis, errors will be introduced, even using ideal radars, because the $\langle |s_{hv}| \rangle^2$ term (called scattering depolarization) couples cross-polar signals to the copolar ones. But, as pointed out by Seliga and Bringi (1976), the coupled cross-polar signal is typically 20 dB below the copolar one and therefore should not seriously affect the method. The decision to test the mode of simultaneously transmitting and receiving H, V waves is rooted in greater expected benefits compared to that obtained with the mode of alternating the transmission and reception of H, V waves. Assuming no propagation effects, the benefits of the simultaneous transmission mode are the following:

- 1) The copolar correlation magnitude $|\rho_{vv}(0)|$ between H and V weather signals at zero lag can be estimated directly. (That is, there is no need to assume a correlation model, nor is there any need to perform the time-consuming spectral calculations if a model is not assumed; Zrnić et al. 1994.)
- 2) The differential phase shift ϕ_{DP} can be estimated directly (i.e., no need to account for Doppler shifts), and therefore, its unambiguous interval of 360° is twice the interval if H, V waves are alternately transmitted and received.
- 3) The unambiguous velocity interval depends only on sample spacing because Doppler velocity estimation is decoupled from ϕ_{DP} estimation.
- 4) There are no compromises in the performance of the ground clutter filter.
- 5) There are fewer errors in polarimetric variables for the same scan rates because the number of samples for each polarized component is doubled.
- 6) There is no need for a costly (>\$100K) high-power ferrite switch in which the power loss is often more than 1.5 dB, exceeding the 1.5-dB reduction in the effective SNR incurred with the simultaneous mode (Doviak et al. 1998).
- 7) First and second trip velocity measurements are assumed.
- 8) There is total compatibility with current WSR-88D processing, ground clutter filtering, and range-velocity ambiguity mitigation solutions.

Alternate transmission of H, V waves has the following benefits:

- 1) Automatic suppression of overlaid echoes from even trip (2d, 4th, . . .) reflectivities.
- 2) The depolarization ratio can be measured.

- 3) There is no need to have a second receiver. (This eliminates the need for matching the two receivers.)

Ryzhkov and Zrnić (1998) made a theoretical comparison of the errors in estimating the polarimetric variable ϕ_{DP} for H, V waves alternately transmitted and received (as copolar signals) with a mode in which H, V waves are simultaneously transmitted. They conclude that the simultaneous transmission of H, V waves provides for reduced statistical fluctuations. This advantage is more pronounced if normalized (to the unambiguous velocity interval) Doppler spectrum widths are larger than 0.1, values that are typically encountered in severe storms observed with the WSR-88D. Clearly, the benefits of simultaneous transmission outweigh the benefits of alternate transmission for most expected operational applications. In section 5, we analyze some of the possible biases in polarimetric variables if H, V polarized waves are simultaneously transmitted.

5. Effects of angular orientation of the feed, drop canting, and backscatter depolarization on polarimetric measurements using simultaneous transmission of H, V waves

Radar measurements of hydrometeors' intrinsic polarimetric parameters (e.g., differential reflectivity, specific differential phase, etc.) sometimes involve unwanted coupling between the H and V waves. This coupling can be caused by inadequate isolation between the two channels (e.g., rotation of the dual-port feed and lack of isolation in other microwave components) and/or canting of the raindrop's axis of symmetry, which can create errors in the parameter estimates. Coupling effects could be especially detrimental if H, V waves are simultaneously transmitted and received. For example, Sachidananda and Zrnić (1985) show that bias errors in differential reflectivity can be an order of magnitude larger for estimates made using H, V polarized waves that are simultaneously transmitted and received rather than alternately transmitted and received. The purpose of this section is to extend the study to other polarimetric parameters and to determine the practical bounds on parameter estimation errors caused by effects such as canting angle dispersion, feed rotation, and backscatter depolarization. Toward this goal, we consider separately the effects of feed rotation, drop canting along the propagation path, and depolarization upon backscattering.

a. Effects of angular orientation of the feed about the focal axis

Consider a dual-port feed that can radiate and receive waves that are either horizontally or vertically polarized if the feed is properly oriented. One port, called the H' port, is assumed to generate and receive linearly polarized waves that are nominally horizontal; likewise, the

V' port generates and receives nominally vertically polarized waves. The primes are used to differentiate the directions H', V', which are shifted by α degrees (the angular displacement of the feed about the focal axis) from the exactly horizontal H and vertical V directions. The H' and V' polarized waves are assumed to be 1) simultaneously transmitted, 2) orthogonal to each other, 3) of equal magnitudes, and 4) having a phase difference β (i.e., $E_{v'} = E_{h'} e^{j\beta}$). Thus, the transmitted wave's polarization is linear if $\beta = 0$ or π , circular (right or left handed) if $\beta = \pm\pi/2$, or elliptical for any other β ; but the tilt angle τ of the polarization ellipse will always be $\pm\pi/4$ plus α relative to the H axis. Furthermore, the radar must be calibrated so that in the absence of propagation effects (e.g., differential attenuation), the voltages $V_{h'}$, $V_{v'}$ in the H' and V' channels of the receiver contributed by a spherical scatterer are identical. Such calibration is needed to ensure that Z_{dr} estimates are not biased. The single subscript h (or v) is used to denote the reception of the horizontally (or vertically) polarized wave if both are transmitted simultaneously.

In practice, it is difficult to control β because it is a function of the differential phase path length within the radar. The KOUN has relatively long waveguides of unequal length for the H and V polarized signals that pass through both the azimuth and elevation rotary joints. Adjusting and keeping the phase paths fixed to achieve a known value of β is a challenging engineering problem. Fortunately, knowing β is not necessary to obtain the desired polarimetric variables, as will be explained shortly.

For sake of simplicity, ignore differential attenuation and assume no coupling between the horizontally and vertically polarized fields as they propagate through precipitation. The effects due to this coupling are discussed in section 5b. The primary reason these assumptions are made is to isolate completely the effects of angular displacement of the feed from all other effects.

For the same reason, we assume there is insignificant phase shift upon backscatter (i.e., $\delta_{hh} = \delta_{vv} = 0$), and that drops are of the same size and are not canted within the sampled V_6 . The effect of canting is discussed in section 5c. Because all drops are of the same size and shape, the $V_{h'}$, $V_{v'}$ signal fluctuations, due to random differential motions of the scatterers in the resolution volume, are perfectly correlated (i.e., $|\rho_{hv}(0)| = 1$). Otherwise, the term $\langle s_{hh}^* s_{vv} \rangle$ would appear in the final expressions requiring introduction of $\rho_{hv}(0)$ which, for rain media, is practically 1 anyway. In the following sections, we present and discuss the results of formulas, derived in the appendix, which describe the bias errors incurred when measuring various polarimetric variables with H, V waves simultaneously transmitted.

1) EFFECTS OF FEED ORIENTATION ON Z_{DR} MEASUREMENTS

The bias in Z_{DR} [appendix Eq. (A7)] is plotted in Fig. 7 for an intrinsic value of $Z_{DR} = 3$ dB and $\alpha = 0.1^\circ$

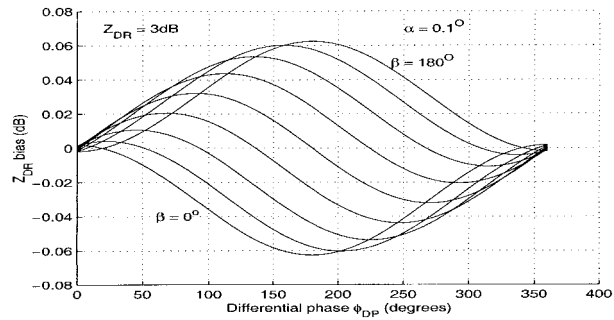


FIG. 7. The differential reflectivity bias (in dB), due to an angular displacement $\alpha = 0.1^\circ$ of the feed about the focal axis vs the round-trip differential phase shift for various values of the differential phase shift β (in steps of 22.5°) upon transmission. The intrinsic differential reflectivity Z_{DR} is assumed to be 3 dB.

(measurements reported in section 3b indicate that, for the KOUN, $\alpha \leq 0.1^\circ$) for various values of β . It is noteworthy that the bias is periodic in ϕ_{DP} and has a maximum excursion of ± 0.062 dB at 180° of differential phase shift if $\beta = \pm 180^\circ$.

It can be shown that for small α , the bias error is proportional to α ; a 1° rotation results in a maximum 0.62-dB bias error at $\phi_{DP} = 180^\circ$. But, with ϕ_{DP} as large as 180° , there would also be significant differential attenuation that needs to be taken into account. For example, Bringi et al. (1990) compute a differential attenuation of about 0.6 dB for a 180° differential phase shift in rain, and Ryzhkov and Zrnic (1995) observed differential attenuation of about 1.6 dB along a path with 180° of differential phase.

In summary, although there is differential reflectivity bias due to angular orientation of the feed about its axis, this bias could be made negligible if the angular displacement α of the feed is kept below a few tenths of a degree. Larger angular displacements of the feed might be tolerated, however, because, at large differential phase shifts, the effects of angular orientation would be masked by other effects (e.g., differential attenuation). On the other hand, if α and β are known, the bias can be removed. Nevertheless, we recommend that angle errors of the feed be constrained to less than about $0.1^\circ - 0.2^\circ$. Because the magnitude of the circular components are unaffected by angular displacement of the (H, V) axis, Fig. 7 demonstrates that Z_{DR} bias is smallest if circularly polarized waves are transmitted (i.e., $\beta = \pm 90^\circ$).

2) EFFECTS OF ANGULAR DISPLACEMENT ON DIFFERENTIAL PHASE MEASUREMENTS

Figure 8 shows the ϕ_{DP} bias, plotted from (A10), as a function of ϕ_{DP} for $\alpha = 1^\circ$, $\gamma = 0^\circ$, Z_{DR} ranging from -1 to $+3$ dB, and $\beta = 40^\circ$, where γ is the differential phase shift between the H, V receivers. Although negative values of ϕ_{DP} do not occur for rain, we have plotted

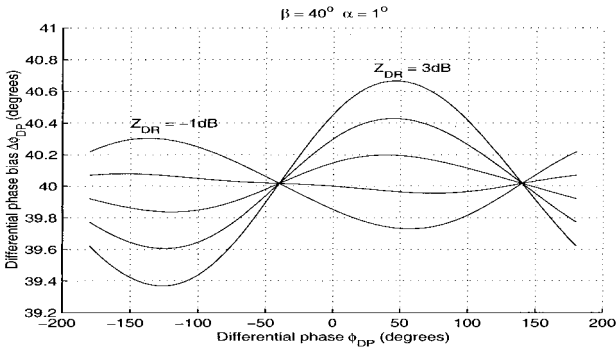


FIG. 8. The differential phase bias, due to the feed's angular offset $\alpha = 1^\circ$, and Z_{DR} ranging from -1 to $+3$ dB in 1-dB steps. The differential phase shift γ within the receiver is assumed to be zero, and $\beta = 40^\circ$.

negative values for convenience because the curves are periodic. From (A10a) it is obvious that γ adds a fixed bias to $\langle \hat{\phi}_{DP} \rangle$, which can be removed through calibration. The oscillatory excursion about β is almost the same for all values of β . But the mean bias β is not important because the parameter of interest is the range gradient of ϕ_{DP} (i.e., K_{DP}) because it is related to the measurements of rainfall rate. It is next demonstrated, however, that the rainfall bias is insignificant.

Consider that, for a moderate rain rate of 37 mm h^{-1} , the one-way specific differential phase change is about 1° km^{-1} [Doviak and Zrnić 1993, their Eq. (8.31a)], Z_h computes to 48 dBZ if the Marshall–Palmer rainfall rate formula is used, and $Z_{DR} = 2.2 \text{ dB}$ [Doviak and Zrnić 1993, their Eq. (8.67)]. From Fig. 8, we see the maximum slope of the differential phase bias occurs over the interval of differential phase from -100° to $+25^\circ$ which, for the cited rain rate, corresponds to a one-way pathlength of 62.5 km. The two-way differential phase bias over this pathlength is about 0.8° ; thus, the specific differential phase bias (one way) is less than $0.0064^\circ \text{ km}^{-1}$. Hence, the bias in rain rate measurements is less than a few tenths of a millimeter per hour; it will be much smaller if the feed's angular offset is significantly less than 1° .

3) ANGULAR DISPLACEMENT EFFECTS ON $|\rho_{hv}(0)|$

In this case, we assume the scatterers are nonspherical but are statistically isotropic and may have a distribution of sizes. An example of such scatterers is tumbling hailstones that on average appear to be spherical and, thus, have $Z_{dr} \approx 1$ ($Z_{DR} = 0 \text{ dB}$), and yet $|\rho_{hv}(0)|$ can be significantly less than 1. For example, if $\alpha = 1^\circ$ and $|\rho_{hv}(0)| = 0.9$, Doviak et al. (1998) demonstrate that the bias error $\Delta\rho_{hv}(0)$ is less than 4×10^{-4} and thus is insignificant.

b. Effects of canting of drops along the propagation path

Canting of raindrops occurs in regions of strong wind shear. Because strong wind shear in thunderstorms is confined to relatively small regions (compared to the propagation pathlength), and because the shear in these regions has (on average) no preferential direction with respect to the direction to the radar, we expect the average canting angle (i.e., the average over the propagation path) to be zero.

Strong shear over large regions often can be found, however, near the ground. In such conditions, raindrops can experience persistent canting. Brussard (1976) demonstrates that the canting is most pronounced close to the ground where shear is usually the strongest; canting as much as 10° has been observed at heights of 10 m above the ground, but at about 80 m, where shear is weaker, a much smaller value of 2° has been reported. For a linear wind profile with the horizontal wind u and vertical shear du/dz , the canting angle ψ , obtained from Brussard (1976), is

$$\tan\psi = \frac{(w_t - w) du/dz}{g}, \quad (19)$$

where $w_t - w$ is the fall speed of the drop, w_t is its terminal velocity, w is the vertical velocity of air, and g is the force of gravity. Given that 9 m s^{-1} is about the upper limit of the terminal velocity of the largest drops, and if $w = 0$ (as it would be near the ground), the canting angle is less than 0.6° for the extremely large shear of 0.01 s^{-1} . Furthermore, the radar beam is typically well above 100 m, and shear in rain at these altitudes is rarely so persistent and strong.

Canting is not only caused by shear. For example, if spatially uniform horizontal wind is accelerating, there will be a relative flow in the direction of acceleration due to the inertia of the drop. Thus, the drop will cant to have its axis of symmetry parallel to the relative flow. Accelerating air on thunderstorm scales is commonly associated with turbulence; hence, accelerations are spatially and temporally random with zero mean. Therefore, drops are momentarily canted one way and then another so that, on average, the canting angle induced by turbulence is zero.

Since the effects of mean canting are exactly the same as the feed's angular offset (e.g., a 1° canting angle produces the same magnitude of Z_{DR} bias as a 1° offset; Doviak et al. 1998), the effects of mean canting on differential phase and copolar correlation magnitude can be determined by referring to sections 5a(2), 5a(3). Thus, we restrict further discussion to the effects of canting angle dispersion.

A random variation of canting angles causes the ensemble of drops to appear less oblate and will decrease the differential phase due to propagation and indirectly bias the measurements of other intrinsic parameters, even if the mean canting angle is zero. Inspection of

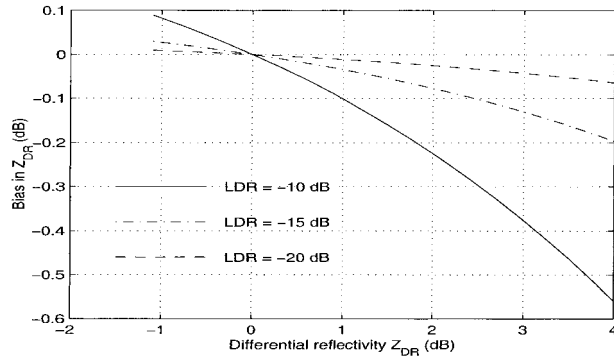


FIG. 9. The bias in Z_{DR} measurements due to depolarization upon backscatter vs the intrinsic differential reflectivity for three values of the linear depolarization ratio (LDR); $\beta = 0^\circ$ and $\alpha = 0^\circ$.

(3) reveals that the dispersion of canting angles decreases the phase shift of the vertically polarized waves, whereas it increases the phase shift of the horizontally polarized wave. The net result is that the propagation differential phase will decrease from the value it would have had if the dispersion were zero.

The decrease, in the expected value of the differential phase $\langle \hat{\phi}_{DP} \rangle$, due to canting angle dispersion will alter the biases in measurements of Z_{DR} , K_{DP} , and $|\rho_{hv}|$. The effect of canting angle dispersion can be determined by moving along any of the curves corresponding to a decrease of ϕ_{DP} by an amount equal to $2\sigma_\psi^2 \phi_{DP}$. It should be pointed out, however, that this bias is also present in measurements using alternately transmitted polarizations. Based upon measurements made with the CSU-CHILL (Universities of Chicago and Illinois) radar using alternate transmissions of H, V waves, canting angle dispersion σ_ψ is estimated to be $\leq 10^\circ$ – 12° and, thus, does not appear to be a significant contributor to errors in measurement.

c. Effects due to depolarization upon backscatter

In the next few paragraphs, we examine the effects that depolarization upon backscatter has on measurement of Z_{dr} , ϕ_{DP} , and $|\rho_{hv}(0)|$.

1) BACKSCATTER DEPOLARIZATION EFFECTS ON Z_{DR}

In Fig. 9, $\langle Z_{dr} \rangle / Z_{dr}$ [in decibels from (A17)] is plotted to indicate the bias in the \hat{Z}_{DR} measurements as a function of the intrinsic Z_{DR} . For significant hail, Z_{DR} is about 0 dB, and there is no bias. But in hail mixed with rain, or in the melting layer, there would be substantial negative bias. For example, if $LDR = -20$ dB and $Z_{DR} = 3$ dB, the bias is less than -0.05 dB but is almost 0.4 dB if LDR increases to the unusually large value of -10 dB. In a severe hailstorm with golf ball-sized hail, Hubbert et al. (1998) found that maximum LDR to be less than -16 dB.

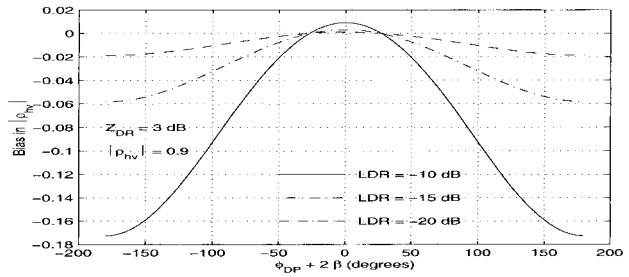


FIG. 10. The $|\rho_{hv}(0)|$ bias, due to backscatter depolarization, vs $2\beta + \phi_{DP}$ for three values of the linear depolarization ratio (LDR); $\alpha = \gamma = 0^\circ$.

2) BACKSCATTER DEPOLARIZATION EFFECTS ON $|\rho_{hv}(0)|$ AND ϕ_{DP}

The bias in estimates $|\hat{\rho}_{hv}(0)|$ is obtained from (A20) and plotted in Fig. 10, and the bias in $\hat{\phi}_{DP}$ is given by (A21) and is plotted in Fig. 11 as a function of $\phi_{DP} + 2\beta$. The bias in correlation magnitude is not very significant if LDR is less -15 dB. Also, the bias in K_{DP} will not be significant, as can be deduced from the following argument. Referring to Fig. 11, it is seen that at an LDR of -15 dB, there is a change of differential phase bias of about 6° per 180° of differential phase change. Assuming a 1° km^{-1} specific differential phase shift produced by rain, it can be deduced that the K_{DP} bias would be about $0.03^\circ \text{ km}^{-1}$. This corresponds to about a 1 mm h^{-1} bias in a rain rate of 37 mm h^{-1} .

6. Comparison of data obtained with simultaneous and alternate transmissions

Because hardware modifications to cycle between the two modes are substantial, no comparisons between the proposed mode of simultaneous transmission and reception of H, V signals and the often used alternate H, V transmission and reception mode (i.e., the HV mode) have been reported in the literature. Perhaps the initial success of the alternate scheme negated the need (at least for scientific purposes) to explore less costly alternatives. Within the last year, the CSU-CHILL staff and scientists

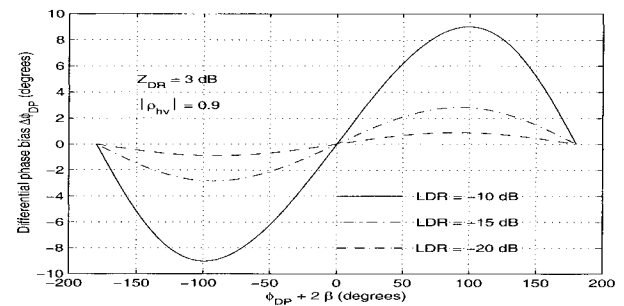


FIG. 11. The differential phase bias due to backscatter depolarization vs $2\beta + \phi_{DP}$ for three values of the linear depolarization ratio (LDR); $\alpha = \gamma = 0^\circ$.

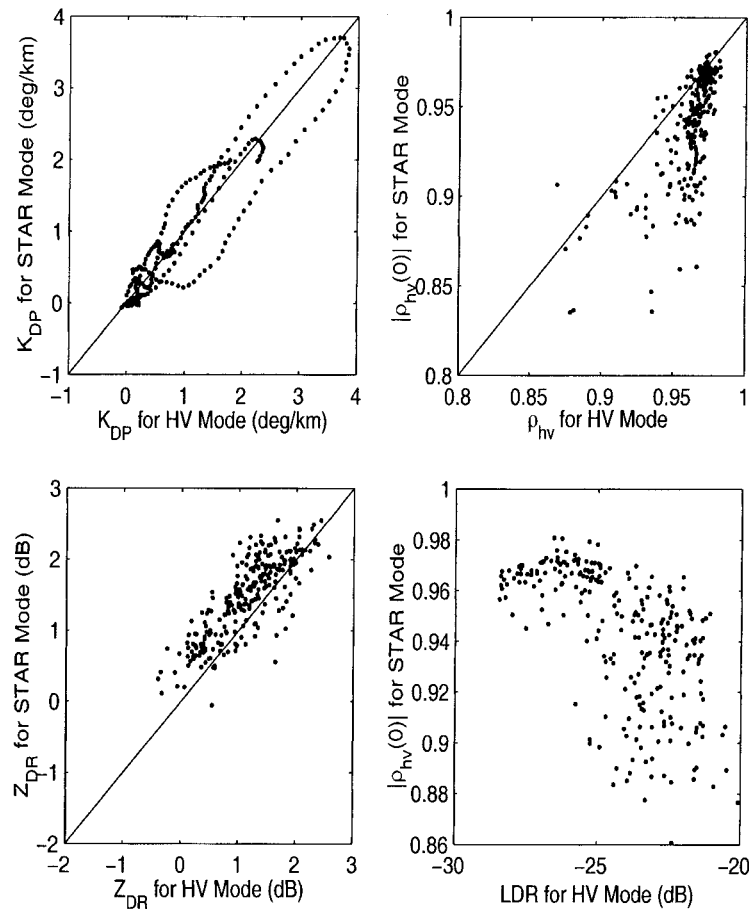


FIG. 12. Scattergrams comparing data collected in the STAR and HV modes. Panels show intercomparisons of K_{DP} , Z_{DR} , and $|\rho_{hv}(0)|$. The lower right panel shows $|\rho_{hv}(0)|$ STAR data vs LDR collected in the HV mode. Data are from a hailstorm observed with CSU's polarimetric Doppler weather radar (CSU-CHILL).

at Colorado State University have implemented the capability to simultaneously transmit the H, V waves, but to alternately receive these in a single receiver channel through the use of a low-power transfer switch; this mode of operation is coined STAR (Simultaneous Transmission Alternate Reception). More recently, data were collected in the simultaneous transmission and simultaneous reception (STSR) mode with two receivers.

Figure 12 presents data, collected with the CSU-CHILL radar when alternating scans in the STAR and the HV mode, that illustrate the *potential* of operating in the mode in which H, V waves are both transmitted and received simultaneously (i.e., the STSR mode). That is, the effects of any feed rotation, canting angle, and backscatter depolarization on the measurements of polarimetric variables (e.g., Z_{DR}) could be made evident in this comparison. These data are from a hailstorm that likely presents the most demanding conditions for comparison. Because the data were collected in scans separated by about 1 min, changes in a rapidly developing

storm could account for some of the observed differences seen in the following figures.

Scattergrams (Fig. 12) of the K_{DP} , $|\rho_{hv}(0)|$, and Z_{DR} demonstrate strong correlation between the parameters estimated from measurements in these two modes. Data were collected at an elevation angle of 0.7° in a region of the hailstorm where Z was relatively uniform. Each point in Fig. 12 is an average of data from 10 resolution volumes spanning an azimuthal arc of about 7° . The path of K_{DP} pairs in Fig. 12 depicts progression as a function of range. Although the average of K_{DP} data is not biased [consistent with the theoretical calculations presented in sections 5a(2), 5b(2), and 5c(2)], and the path of K_{DP} data exhibits a cyclic bias (two cycles of bias are seen in this figure corresponding to the two rain cells seen in Fig. 13) suggested by theory (i.e., Figs. 8 or 11), there are unexpectedly large biases (i.e., $\pm 0.5^\circ \text{ km}^{-1}$); further research is required to explain this difference. The Z_{DR} in the STAR mode is higher by about 0.2 dB (Fig. 12b), which is most likely due to a slight mismatch in the power

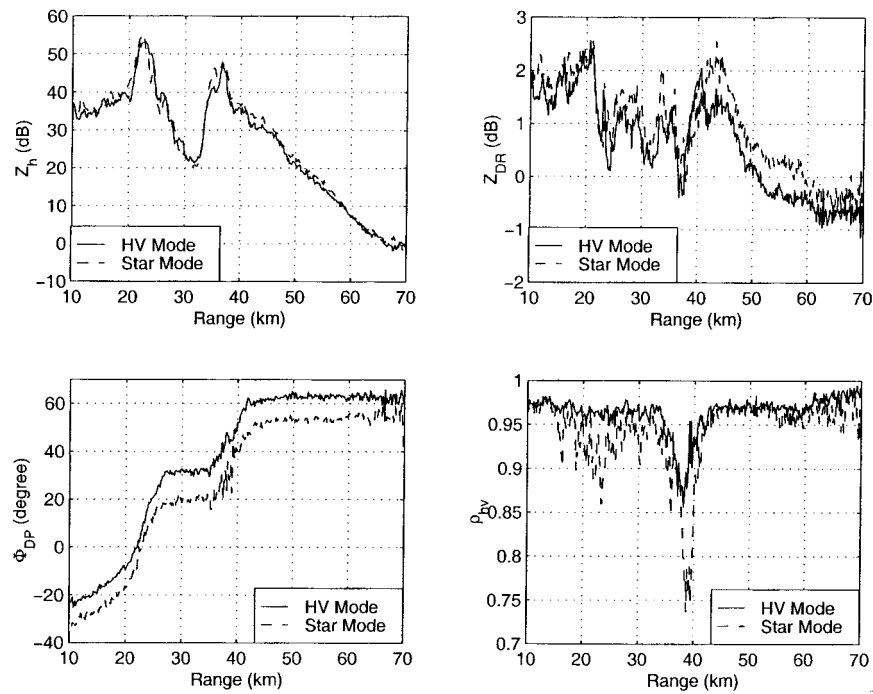


FIG. 13. Radial profiles of Z_h , Z_{DR} , ϕ_{DP} , and $|\rho_{hv}(0)|$ at a single azimuth for the storm, which supplied data presented in Fig. 12.

emitted by the two transmitters; this mismatch can be removed through calibration. The correlation $|\rho_{hv}(0)|$ in the STAR mode is lower than in the alternate mode; this is consistent with the composite effects of factors discussed in sections 5a(3), 5b(3), and 5c(2). The $|\rho_{hv}(0)|$ in the STAR mode versus LDR in the HV mode (Fig. 12d) further demonstrates that the bias in $|\rho_{hv}(0)|$ is likely due to scattering depolarization (i.e., where LDR is high).

Radial profiles of Z_h , Z_{DR} , ϕ_{DP} , and $|\rho_{hv}(0)|$ are displayed in Fig. 13. The correspondence between the reflectivity factors Z_h and differential phases ϕ_{DP} for the

two modes is remarkable. The offset between the two ϕ_{DP} curves is due to the difference in system phases, and it does not affect the estimation of rainfall rate. The lower values of $|\rho_{hv}(0)|$ data collected in the STAR mode are consistent with theory suggesting that these would accentuate the contrast between hail and rain. The bias in Z_{dr} could be caused by about a 1° rotation of the feed. The relatively constant Z_{dr} bias for ranges between 45 and 60 km is consistent with the relatively constant ϕ_{DP} in this range interval.

Figure 14 shows a comparison of data collected in the HV and STSR modes in another storm. The data are vertical profiles of the observations constructed from elevation scans at the same azimuth angle but separated in time by 30 s. Data between the ranges of 85–88 km are averaged. This range interval was chosen to bracket the most intense part of the storm. Good agreement between data collected in the two modes is noted for the most part, although there appear to be small pervasive differences in Z_{DR} , K_{DP} , and $|\rho_{hv}(0)|$ at low altitudes; further research is required to pinpoint the cause of these differences.

Overall, these measurements indicate that simultaneous transmission and reception of H, V waves (i.e., the STSR mode) should produce at least as good as or, perhaps, better results than the STAR or HV modes. That is, because reception in either the STAR or HV mode alternates between H and V signals, the Doppler spread degrades estimates of the parameters Z_{DR} , ϕ_{DP} , and $|\rho_{hv}(0)|$ made in either of these modes. The HV mode

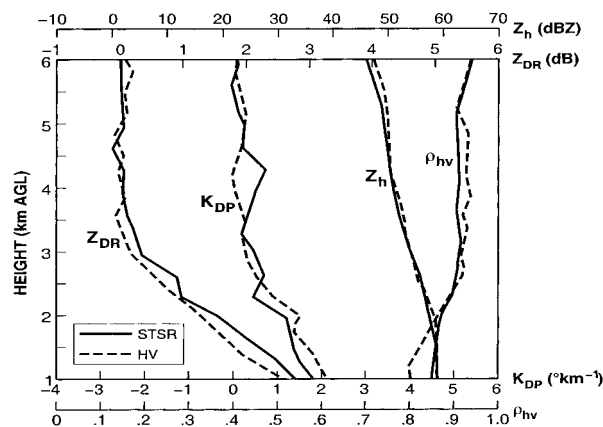


FIG. 14. Vertical profiles of radar measurements in HV and STSR modes separated by about 30 s. Data were collected in elevation scans at the same azimuth through the core of a convective storm.

data agree much better with the STSR mode data, perhaps because the STSR mode allows direct computation and more accurate estimates of the polarimetric parameters.

7. Summary and conclusions

An examination is made of several considerations required before a polarimetric upgrade is added to the WSR-88D radar to improve rainfall rate measurements. An engineering evaluation was made to determine if the existing antenna assembly of the WSR-88D (NEXRAD) could be used as is for the dual-polarization mode. It was meant to guide us in the selection of hardware for upgrading the WSR-88D to polarimetric capability. The current assembly has a feed supported by three struts, which presents a blockage of radiation that differently affects the horizontally and vertically polarized fields. On the other hand, the sidelobes of the antenna with the three struts are significantly lower than the sidelobes of antennas having four struts used in high quality polarimetric research. Thus, we recommend no change in feed support struts.

A dual-port antenna feed was purchased from Andrew Canada, Inc., and installed on the radar. Pattern measurements were made for the horizontal and vertical polarizations in the horizontal plane and for both polarizations in the lower half of the vertical plane. Note that the secondary radiation patterns with the dual-port feed are very close to the patterns measured with the single-port feed on the unmodified WSR-88D. Both copolar patterns have low sidelobe levels and are well matched in the main lobe. Beamwidths are 0.93° for the horizontal copolar and 0.90° for the vertical copolar patterns. The match of patterns in the lower half of the vertical plane is excellent; it even extends to several of the sidelobes. We have also examined contours of the power ratio (horizontal/vertical in dB) where the antenna gain, relative to the boresight gain, is larger than -20 dB. For the most part, the patterns agree to within ± 1 dB.

Cross-polarization patterns were also recorded, and it was observed that the cross-polar peak in the horizontal copolar channel is more than 35 dB below the copolar peak. The cross-polar pattern at vertical polarization roughly matches the cross-polar pattern at horizontal polarization, but the amplitudes appear to be a few decibels higher. This could be due to limitations of our ad hoc antenna range.

Considerations for the choice of polarimetric basis and a few system design options are described in section 4, where the circular and linear polarimetric bases are compared. Although a circular basis can provide estimates of specific differential phase (K_{DP}) without switching the transmitted polarization, these estimates are corrupted in stratiform rain because the cross-polar signal is almost three orders of magnitude below the copolar signal. With circular polarization, the cross-po-

lar signal does not depend on the orientation of hydrometeors and, in combination with the copolar signal, it leads to direct measurement of the mean canting angle. Nonetheless, these apparent advantages of the circular polarization basis diminish in the presence of significant precipitation along the radar beam. The linear polarization basis is well suited for quantitative measurement of rainfall and classification of hydrometeor types without extensive correction of propagation effects. Moreover, it still provides measurements from which some circular polarization parameters (e.g., the circular depolarization ratio) can be obtained. Therefore, our choice rests with the linear H, V basis.

A polarimetric scheme employing simultaneous transmission and reception of horizontally and vertically polarized waves is being implemented on NSSL's research WSR-88D. This design includes the installation of two receivers that share several common components, but a single receiver can also measure the polarimetric variables. With simultaneous transmission, the depolarization ratio cannot be measured with other polarimetric variables; nonetheless, if desired, it can be measured together with the standard spectral moments in separate volume scans. With two receivers, the dwell time for computing polarimetric variables is reduced, and the ground clutter filter is not affected. Having two receivers also offers some redundancy that might be advantageous. For comparative testing, the NSSL plans to incorporate two receivers in its radar and still retain full WSR-88D compatibility. That is, all current data acquisition modes and scanning strategies can remain, and the impact of polarimetric implementation on the existing algorithms and products should be minimal.

Theoretical considerations of feed alignment, drop canting, and backscatter depolarization suggest that using simultaneous transmission of H and V signals would allow accurate measurements of specific differential phase K_{DP} , the principal polarimetric parameter which should lead to improved rainfall measurements. Overall, Z_{DR} is much more affected by simultaneous transmission than the other polarimetric parameters. Results (Fig. 7) demonstrate that the transmission of circularly polarized waves reduces the overall bias in Z_{DR} (i.e., by fixing the phase angle β , the angle between the transmitted H and V waves, to be $\pm 90^\circ$). If feed rotation errors are less than a few tenths of a degree, the errors in Z_{DR} are small, so there is no need to determine or set β . But if rotation errors are significant, β needs to be determined to remove the bias in Z_{DR} .

Accurate measurements of the magnitude and phase ϕ_{DP} of the correlation coefficient $\rho_{hv}(0)$ between copolar signals can be maintained if feed rotation α is less 1° , whereas Z_{DR} requires α to be no more than about 0.1° to 0.2° ; this alignment accuracy has been achieved with a dual-port feed installed on the research WSR-88D radar. If differential phase $\phi_{DP} \approx 180^\circ$ (i.e., if propagation is over long paths filled with heavy rain), uniform canting of 1° along the propagation path would significantly bias Z_{DR} (Fig. 7) but would not be detrimental to the mea-

surement of $|\rho_{hv}(0)|$ and K_{DP} . On the other hand, differential attenuation would be significant at these large values of ϕ_{DP} and is a problem whether H, V waves are transmitted simultaneously or alternately. Differential reflectivity is affected by depolarization due to backscattering from hail mixed with rain, and the correlation coefficient is also affected. But backscatter depolarization would accentuate the signatures of low Z_{DR} and low $|\rho_{hv}(0)|$ in hail regions (i.e., reduce even more the low values of Z_{DR} and ρ_{hv} in these regions). Thus, the effect might be beneficial from an operational viewpoint.

Acknowledgments. The contributions of J. Carter, M. Schmidt, S. Torres, and R. Wakinney are greatly appreciated. J. O'Bannon drafted some of the figures, and M. Frazier edited the manuscript; D. Brunkow of the CSU-CHILL staff was responsible for implementing the simultaneous transmission technique. The CSU-CHILL radar is supported by a cooperative agreement with the National Science Foundation via ATM-9500108. The contributions of V. N. Bringi were supported by the U.S. Weather Research Program via the NSF/ATM-9612519. The work on the open RDA is supported by the Office of Systems Development of the NWS.

APPENDIX

Effects on Polarimetric Measurements with Simultaneous Transmission and Reception of H, V Waves

a. Feed rotation

If \mathbf{V}' and \mathbf{E}' are column vector representations of the signals $V_{h'}$, $V_{v'}$ in the receiver and the transmitted fields $E_{h'}$, $E_{v'}$ at the antenna, \mathbf{V}' and \mathbf{E}' are linearly related by the transformation

$$\mathbf{V}' = \mathbf{A}\mathbf{R}'\mathbf{T}'\mathbf{S}\mathbf{T}\mathbf{R}\mathbf{E}', \quad (\text{A1})$$

where the receiver transfer matrix \mathbf{A} is

$$\mathbf{A} = \begin{bmatrix} e^{j\gamma} & 0 \\ 0 & 1 \end{bmatrix}, \quad (\text{A2})$$

and the rotation matrix \mathbf{R} is

$$\mathbf{R} = \begin{bmatrix} \cos\alpha & -\sin\alpha \\ \sin\alpha & \cos\alpha \end{bmatrix}. \quad (\text{A3})$$

where α is the angular displacement (rotation) of the feed about its axis and γ is the differential phase between the H and V receivers. The specific form of \mathbf{R} given by (A3) implies that the coupling between the H and V fields is caused by rotation of an otherwise perfect feed (i.e., one without coupling between the H and V ports). The receiver transfer matrix implies no coupling between channels and equal gains, but a phase difference of γ . We have ignored the changes of signals with range, attenuation, and proportionality constants that make (A1) dimensionally correct. We also assume H, V radiation patterns are matched and that there is negligible coupling between the H and V ports of the antenna; the coupling is less than -40 dB (Doviak et al. 1998, his section II.3). Effects of pattern mismatch, both in amplitude and phase, and coupling are discussed by Chandrasekar and Keeler (1993).

The expected value of the measured differential reflectivity $\langle \hat{Z}_{dr} \rangle$ can be expressed as the ratio

$$\langle \hat{Z}_{dr} \rangle = \frac{\langle |\hat{V}_{h'}|^2 \rangle}{\langle |\hat{V}_{v'}|^2 \rangle}. \quad (\text{A4})$$

Solving for $V_{h'}$, $V_{v'}$ from (A1) and inserting it into (A4) produces the following:

$$\langle \hat{Z}_{dr} \rangle = \frac{|s_{hh}e^{-j\phi_{DP}} \cos^2\alpha + s_{vv} \sin^2\alpha - (s_{hh}e^{-j\phi_{DP}} - s_{vv})e^{j\beta} \sin\alpha \cos\alpha|^2}{|s_{hh}e^{j(\beta-\phi_{DP})} \sin^2\alpha + s_{vv}e^{j\beta} \cos^2\alpha - (s_{hh}e^{-j\phi_{DP}} - s_{vv}) \sin\alpha \cos\alpha|^2}. \quad (\text{A5})$$

Because drops within the sampled resolution volume are assumed to have the same size and shape, the expectation operation need not appear in (A5). Only the portion $E_{v'} \sin\alpha$ of the vertical component is added to the horizontal component, and hence, only the phase of this portion is differentially shifted by propagation. Thus, the phase difference β between the H' and V'

waves at the transmitter does not simply add to the differential phase due to propagation.

If the intrinsic differential reflectivity Z_{dr} is used in place of s_{hh}/s_{vv} in (A5) to obtain the Z_{DR} (dB scale) bias, ΔZ_{DR} , from

$$\langle \hat{Z}_{DR} \rangle = Z_{DR} + \Delta Z_{DR}, \quad (\text{A6})$$

the bias ΔZ_{DR} (in dB) is given by

$$\Delta Z_{DR} = 10 \log_{10} \left[\frac{|e^{-j\phi_{DP}}(\cos^2\alpha - e^{j\beta} \sin\alpha \cos\alpha) + (\sin^2\alpha + e^{j\beta} \sin\alpha \cos\alpha)(Z_{dr})^{-1/2}|^2}{|e^{-j\phi_{DP}}(e^{j\beta} \sin^2\alpha - \sin\alpha \cos\alpha)(Z_{dr})^{1/2} + e^{j\beta} \cos^2\alpha + \sin\alpha \cos\alpha|^2} \right]. \quad (\text{A7})$$

Now, examine the bias in differential phase. Its expected value, $\langle \hat{\phi}_{\text{DP}} \rangle$, is defined as

$$\langle \hat{\phi}_{\text{DP}} \rangle = \arg(\langle \hat{V}_h^* \hat{V}_v \rangle). \quad (\text{A8})$$

Because V_h, V_v are perfectly correlated under assumptions given in section 5a, $\langle \hat{\phi}_{\text{DP}} \rangle$ for the ensemble of scatters is identical to that for a single scatterer. Therefore, if $\alpha = 0$,

$$\langle \hat{\phi}_{\text{DP}} \rangle = \beta - \gamma + \phi_{\text{DP}}, \quad (\text{A9})$$

where $\beta - \gamma$ is the contribution to the measured differential phase caused by differential phase shifts in the transmitter and receiver, and ϕ_{DP} is the intrinsic phase difference.

The differential phase bias is defined as $\Delta\phi_{\text{DP}} \equiv \langle \hat{\phi}_{\text{DP}} \rangle - \phi_{\text{DP}}$. Using (A1) to calculate V_h, V_v , for the case $\alpha \neq 0$, and substituting the results of this calculation into (A8), the following equation is obtained:

$$\Delta\phi_{\text{DP}} = -\gamma + \arg(p), \quad (\text{A10a})$$

where

$$\begin{aligned} p = & \sqrt{Z_{\text{dr}}} e^{+j\beta} (\cos^4 \alpha + e^{-j2\phi_{\text{DP}}} \sin^4 \alpha) \\ & - \sqrt{Z_{\text{dr}}} e^{-j\beta} \sin^2 \alpha \cos^2 \alpha (1 + e^{-2j\phi_{\text{DP}}}) \\ & + e^{-j\phi_{\text{DP}}} \sin \alpha \cos \alpha \\ & \times [(1 - Z_{\text{dr}}) + 2(1 + Z_{\text{dr}}) \sin \alpha \cos \alpha \cos \beta]. \end{aligned} \quad (\text{A10b})$$

Next, the bias in measurement of the correlation coefficient magnitude is examined. The magnitude of the expected measurement of the copolar correlation coefficient can be written as

$$|\langle \hat{\rho}_{\text{hv}}(0) \rangle| = |\rho_{\text{hv}}(0)| + \Delta\rho_{\text{hv}}(0), \quad (\text{A11})$$

where

$$\langle \hat{\rho}_{\text{hv}}(0) \rangle = \frac{\langle (\hat{V}_h \hat{V}_v^*) \rangle}{\sqrt{\langle |\hat{V}_h|^2 \rangle \langle |\hat{V}_v|^2 \rangle}}. \quad (\text{A12})$$

Substituting $\mathbf{A} = \mathbf{R} = \mathbf{I}$, the identity matrix, into (A1), one obtains relations to compute the bias.

b. Depolarization upon backscatter

Consider first a single canted scatterer in V_6 , illuminated with horizontally and vertically polarized fields. As before, in order to isolate the effects of depolarization upon backscatter from other effects, we

assume no rotation of the feed (i.e., $\alpha = 0$), and canting angles along the propagation path have a zero mean (i.e., $\psi = 0$). There is a net differential phase between the two polarized components illuminating the scatterer because 1) drops along the propagation path are oblate, and 2) the phase between the two transmitted components is β , and the differential phase in the H, V receivers is γ . Taking these into account and again ignoring radar constants, etc., the corresponding backscatter voltages in the receiver's H and V channels are proportional to

$$\begin{aligned} V_h = & [s_{hh} \exp(-j\Phi_{\text{DP}}/2) + s_{hv} e^{j\beta}] \\ & \times \exp(-j\Phi_{\text{DP}}/2 + j\gamma) \quad \text{and} \\ V_v = & s_{vv} e^{j\beta} + s_{hv} \exp(-j\Phi_{\text{DP}}/2). \end{aligned} \quad (\text{A13})$$

For an ensemble of scatterers having a distribution of sizes and differential phases, the mean detected power, $P_h = \langle \hat{V}_h \hat{V}_h^* \rangle$, in the H receiver is

$$\begin{aligned} P_h = & \langle [s_{hh} \exp(-j\phi_{\text{DP}}/2) + s_{hv} e^{j\beta}] \\ & \times [s_{hh}^* \exp(j\phi_{\text{DP}}/2) + s_{hv}^* e^{-j\beta}] \rangle. \end{aligned} \quad (\text{A14})$$

An expression similar to (A14) can be obtained for the power P_v .

Next we assume that hydrometeors within V_6 have a symmetric distribution of canting angles about a zero mean so that (Jameson and Dave 1988; Ryzhkov 1991)

$$\langle s_{hh} s_{hv}^* \rangle = \langle s_{vv} s_{hv}^* \rangle = 0. \quad (\text{A15})$$

This is also a good assumption for hail, which depolarizes the signal significantly but also causes large cross coupling. Using (A15) in (A14), the ensemble averages for P_h and P_v reduce to

$$\begin{aligned} P_h = & \langle s_{hh} s_{hh}^* \rangle + \langle s_{hv} s_{hv}^* \rangle \quad \text{and} \\ P_v = & \langle s_{vv} s_{vv}^* \rangle + \langle s_{hv} s_{hv}^* \rangle. \end{aligned} \quad (\text{A16})$$

Thus, the expected value of the measured differential reflectivity factor can be expressed as

$$\langle \hat{Z}_{\text{dr}} \rangle = Z_{\text{dr}} \frac{1 + \text{Ldr}}{1 + Z_{\text{dr}} \text{Ldr}}, \quad (\text{A17})$$

where $\text{Ldr} \equiv \langle s_{hv} s_{hv}^* \rangle / \langle s_{hh} s_{hh}^* \rangle$ is due to canting dispersion.

The biases in the copolar correlation, $\langle \rho_{\text{hv}}(0) \rangle$, can be obtained from (A13) by taking appropriate products and expectations. The expected value of the correlation coefficient is calculated to be

$$\langle \hat{\rho}_{\text{hv}}(0) \rangle = \rho_{\text{hv}}(0) \frac{\left[1 + \frac{\langle s_{hv} s_{hv}^* \rangle}{\langle s_{hh} s_{hh}^* \rangle} \exp[-j(\phi_{\text{DP}} + 2\beta)] \right] \exp[j(\phi_{\text{DP}} + \beta)]}{\left[\left(1 + \frac{\langle s_{hv} s_{hv}^* \rangle}{\langle s_{hh} s_{hh}^* \rangle} \right)^{1/2} \left(1 + \frac{\langle s_{hv} s_{hv}^* \rangle}{\langle s_{vv} s_{vv}^* \rangle} \right)^{1/2} \right]}. \quad (\text{A18})$$

Note that (A18) can be written in terms of Ldr and Z_{dr} . To get numerical values, we assume $\delta_\ell = 0$, and express the ratio as

$$\frac{\langle s_{hv} s_{hv}^* \rangle}{\langle s_{hh} s_{vv}^* \rangle} = \frac{\text{Ldr } Z_{dr}^{1/2}}{\rho_{hv}(0)}. \quad (\text{A19})$$

Because $\delta_\ell = 0$, $\langle s_{hh} s_{vv}^* \rangle$ is real, hence, $\rho_{hv}(0)$ is real. With these simplifications, the magnitude of the expected correlation coefficient, $|\langle \hat{\rho}_{hv}(0) \rangle|$, becomes

$$|\langle \hat{\rho}_{hv}(0) \rangle| = \rho_{hv}(0) \frac{\left| 1 + \frac{\text{Ldr } Z_{dr}^{1/2} \exp[-j(\phi_{DP} + 2\beta)]}{\rho_{hv}(0)} \right|}{[1 + \text{Ldr}]^{1/2} [1 + \text{Ldr } Z_{dr}]^{1/2}}, \quad (\text{A20})$$

and its phase is

$$\begin{aligned} \langle \hat{\phi}_{DP} \rangle - \phi_{DP} \\ = \beta + \arg \left[1 + \frac{\text{Ldr } Z_{dr}^{1/2} \exp[-j(2\beta + \phi_{DP})]}{\rho_{hv}(0)} \right]. \end{aligned} \quad (\text{A21})$$

REFERENCES

- Balakrishnan, N., and D. S. Znríc, 1989: Correction of propagation effects at attenuating wavelengths in polarimetric radars. Preprints, *24th Conf. on Radar Meteorology*, Tallahassee, FL, Amer. Meteor. Soc., 287–291.
- , and —, 1990: Use of polarization to characterize precipitation and discriminate large hail. *J. Atmos. Sci.*, **47**, 1525–1540.
- Barge, B. L., 1970: Polarization observations in Alberta. Preprints, *14th Radar Meteorology Conf.*, Tuscon, AZ, Amer. Meteor. Soc., 221–224.
- , 1974: Polarization measurements of precipitation backscatter in Alberta. *J. Res. Atmos.*, **8**, 163–173.
- Beard, K. V., and A. R. Jameson, 1983: Raindrop canting. *J. Atmos. Sci.*, **40**, 448–454.
- Bebbington, D. H. O., R. McGuinness, and A. R. Holt, 1987: Correction of propagation effects in S-band circular polarization-diversity radars. *IEE Proc.*, **134**, 431–437.
- Bringi, V. N., and A. Hendry, 1990: Technology of polarization diversity radars for meteorology. *Radar in Meteorology*, D. Atlas, Ed., Amer. Meteor. Soc., 109–190.
- , V. Chandrasekar, N. Balakrishnan, and D. S. Znríc, 1990: An examination of radar propagation effects in rainfall at microwave frequencies. *J. Atmos. Oceanic Technol.*, **7**, 829–840.
- Brunkow, D. A., P. C. Kennedy, S. A. Rutledge, V. N. Bringi, and V. Chandrasekar, 1997: CSU–CHILL radar status and comparison of available operating modes. Preprints, *28th Conf. Radar Meteorology*, Austin, TX, Amer. Meteor. Soc., 43–44.
- Brussard G., 1976: A meteorological model for rain-induced cross polarization. *IEEE Trans. Antennas Propag.*, **AP-24**, 5–11.
- Chandrasekar, V., and R. J. Keeler, 1993: Antenna pattern analysis and measurements for multiparameter radars. *J. Atmos. Oceanic Technol.*, **10**, 674–683.
- Doviak, R. J., and D. S. Znríc, 1993: *Doppler Radar and Weather Observations*. Academic Press, 562 pp.
- , —, J. Carter, A. Ryzhkov, S. Torres, and A. Zahrai, 1998: Polarimetric upgrades to improve rainfall measurements. Report of the National Severe Storms Laboratory, 110 pp. [Available from NSSL, 1313 Halley Circle, Norman, OK 73069.]
- English, M., B. Kochubajda, F. D. Barlow, A. R. Holt, and R. McGuinness, 1991: Radar measurement of rainfall by differential propagation phase: A pilot experiment. *Atmos.–Ocean*, **29**, 357–380.
- Fradin, A. Z., 1961: *Microwave Antennas*. Pergamon Press, 668 pp.
- Holt, A. R., 1988: Extraction of differential propagation phase from data from S-band circularly polarized radars. *Electron. Lett.*, **24**, 1241–1242.
- Hubbert, J., V. N. Bringi, L. D. Carey, and S. Bolen, 1998: CSU–CHILL polarimetric radar measurement from a severe hailstorm in eastern Colorado. *J. Appl. Meteor.*, **37**, 749–755.
- IEEE, 1983: IEEE standard definitions of terms for antennas. Std 145-1983, 29 pp. [Available from IEEE, Inc., 345 E. 47th St., New York, NY 10017.]
- Jameson, A. R., 1983: Microphysical interpretation of multi-parameter radar measurements in rain. Part I: Interpretation of polarization measurements and estimation of raindrop shapes. *J. Atmos. Sci.*, **40**, 1792–1802.
- , and J. H. Davé, 1988: An interpretation of circular polarization measurements affected by propagation differential phase shift. *J. Atmos. Oceanic Technol.*, **5**, 405–415.
- McCormick, G. C., and A. Hendry, 1975: Principles for the radar determination of the polarization properties of precipitation. *Radio Sci.*, **10**, 421–434.
- McGuinness, R., D. H. O. Bebbington, and A. R. Holt, 1987: Modeling propagation effects in the use of S-band polarization-diversity radars. *IEE Proc.*, **134**, 423–430.
- NEXRAD, 1992: Critical item B2 development specification for antenna pedestal, SCN001. Rep. DV1208252G, 51 pp. [Available from the WSR-88D Support Facility, 3200 Marshal Ave., Norman, OK 73072.]
- Oguchi, T., 1983: Electromagnetic wave propagation and scattering in rain and other hydrometeors. *Proc. IEEE*, **71**, 1029–1078.
- Randall, M., J. Lutz, and J. Fox, 1997: S-Pol's high isolation mechanical polarization switch. Preprints, *28th Conf. on Radar Meteorology*, Austin, TX, Amer. Meteor. Soc., 252–253.
- Ryzhkov, A. V., 1991: Polarimetric information measurements in radar meteorology: Theoretical model (in Russian). *Radioelectron. Commun.*, **2**, 17–23.
- , 1993: Polarization methods in radar meteorology (in Russian). *Foreign Radio Electron.*, **4**, 18–28.
- , and D. S. Znríc, 1995: Precipitation and attenuation measurements at a 10-cm wavelength. *J. Appl. Meteor.*, **34**, 2121–2123.
- , and —, 1996: Assessment of rainfall measurement that uses specific differential phase. *J. Appl. Meteor.*, **35**, 2080–2090.
- , and —, 1998: Polarimetric rainfall estimation in the presence of anomalous propagation. *J. Atmos. Oceanic Technol.*, **15**, 1320–1330.
- Sachidananda, M., and D. S. Znríc, 1985: Z_{DR} measurement considerations for a fast scan capability radar. *Radio Sci.*, **20**, 907–922.
- , and —, 1986: Differential propagation phase shift and rainfall rate estimation. *Radio Sci.*, **21**, 235–247.
- , —, and R. J. Doviak, 1997: Signal design and processing techniques for WSR-88D ambiguity resolution, Part 1. NSSL Report, 100 pp. [Available from NSSL, 1313 Halley Circle, Norman, OK 73069.]
- , —, —, and S. Torres, 1998: Signal design and processing techniques for WSR-88D ambiguity resolution, Part 2. NSSL Report, 105 pp. [Available from NSSL, Norman, OK 73069.]
- Saffie, R. E., L. D. Johnson, 1997: NEXRAD Product Improvement Overview. Preprints, *13th Int. Conf. on Interactive Information and Processing Systems for Meteorology, Oceanography, and Hydrology*, Long Beach, CA, Amer. Meteor. Soc., 223–227.
- Seliga, T. A., and V. N. Bringi, 1976: Potential use of radar differential reflectivity measurements at orthogonal polarizations for measuring precipitation. *J. Appl. Meteor.*, **15**, 69–76.
- , and —, 1978: Differential reflectivity and differential phase shift: Applications in radar meteorology. *Radio Sci.*, **13**, 271–275.

- Spilhaus, A. E., 1948: Raindrop size, shape, and falling speed. *J. Meteor.*, **5**, 108–110.
- Torlaschi, E., and B. Pettigrew, 1990: Propagation effects on reflectivity for circularly polarized S-band radars. *J. Atmos. Oceanic Technol.*, **7**, 114–117.
- , and A. R. Holt, 1993: Separation of propagation and back-scattering effects in rain for circular polarization diversity S-band radars. *J. Atmos. Oceanic Technol.*, **10**, 465–477.
- Zahrai, A., and D. S. Znić, 1997: Implementation of polarimetric capability for the WSR-88D (NEXRAD) radar. Preprints, *13th Int. Conf. on Interactive Information and Processing Systems for Meteorology, Oceanography, and Hydrology*, Long Beach, CA, Amer. Meteor. Soc., 284–287.
- , J. K. Carter, V. Melnikov, and I. Ivic, 1998: The design of a new signal processing subsystem for the WSR-88D (NEXRAD) radar. Preprints, *Int. Conf. on Interactive Information and Processing Systems for Meteorology, Oceanography, and Hydrology*, Phoenix, AZ, Amer. Meteor. Soc., 275–278.
- Zawadzki, I., 1984: Factors affecting the precision of radar measurements of rain. Preprints, *22d Conf. Radar Meteorology*, Zurich, Switzerland, Amer. Meteor. Soc., 251–256.
- Znić, D. S., 1996: Simultaneous differential polarimetric measurements and co-polar correlation coefficient measurements. U.S. Patent Number 5500646, 7 pp.
- , and A. V. Ryzhkov, 1996: Advantages of rain measurements using specific differential phase. *J. Atmos. Oceanic Technol.*, **13**, 454–464.
- , N. Balakrishnan, A. V. Ryzhkov, and S. L. Durden, 1994: Use of correlation coefficient for probing precipitation at nearly vertical incidence. *IEEE Trans. Geosci. Remote Sens.*, **32**, 740–748.